

The RXLR effector PpE18 of *Phytophthora parasitica* is a virulence factor and suppresses peroxisome membrane-associated ascorbate peroxidase NbAPX3-1-mediated plant immunity

Yimeng Cao^{1*} , Qiang Zhang^{2*} , Yuan Liu¹ , Tiantian Yan¹, Liwen Ding¹, Yang Yang^{1,2} , Yuling Meng¹ and Weixing Shan¹ 

¹State Key Laboratory for Crop Stress Resistance and High-Efficiency Production, and College of Agronomy, Northwest A&F University, Yangling, Shaanxi, 712100, China; ²State Key Laboratory for Crop Stress Resistance and High-Efficiency Production, and College of Plant Protection, Northwest A&F University, Yangling, Shaanxi, 712100, China

Summary

Author for correspondence:
Weixing Shan
Email: wxshan@nwfau.edu.cn

Received: 27 December 2023
Accepted: 28 May 2024

New Phytologist (2024) **243**: 1472–1489
doi: 10.1111/nph.19902

Key words: NbAPX3-1, peroxisome, *Phytophthora parasitica*, plant immunity, PpE18, ROS-scavenging activity, RXLR effector.

- *Phytophthora parasitica* causes diseases on a broad range of host plants. It secretes numerous effectors to suppress plant immunity. However, only a few virulence effectors in *P. parasitica* have been characterized.
- Here, we highlight that PpE18, a conserved RXLR effector in *P. parasitica*, was a virulence factor and suppresses *Nicotiana benthamiana* immunity. Utilizing luciferase complementation, co-immunoprecipitation, and GST pull-down assays, we determined that PpE18 targeted NbAPX3-1, a peroxisome membrane-associated ascorbate peroxidase with reactive oxygen species (ROS)-scavenging activity and positively regulates plant immunity in *N. benthamiana*. We show that the ROS-scavenging activity of NbAPX3-1 was critical for its immune function and was hindered by the binding of PpE18. The interaction between PpE18 and NbAPX3-1 resulted in an elevation of ROS levels in the peroxisome.
- Moreover, we discovered that the ankyrin repeat-containing protein NbANKr2 acted as a positive immune regulator, interacting with both NbAPX3-1 and PpE18. NbANKr2 was required for NbAPX3-1-mediated disease resistance. PpE18 competitively interfered with the interaction between NbAPX3-1 and NbANKr2, thereby weakening plant resistance.
- Our results reveal an effective counter-defense mechanism by which *P. parasitica* employed effector PpE18 to suppress host cellular defense, by suppressing biochemical activity and disturbing immune function of NbAPX3-1 during infection.

Introduction

In the natural environment, plants are inevitably threatened by a variety of biotic and abiotic stresses, including the infection of pathogens. Coevolution between host plants and pathogens has resulted in an ongoing arms race in which constantly evolved strategies restrain one another from competing for supremacy (Jones & Dangl, 2006; Wang *et al.*, 2019). Plants evolved two layers of immune system to resist pathogens, which are microbe/damage-associated molecular pattern (MAMP/DAMP)-triggered immunity (PTI) and effector-triggered immunity (ETI) (Jones & Dangl, 2006; Boller & Felix, 2009). To subvert plant defense responses, pathogens utilize diverse strategies, including the secretion of varied effectors that impede PTI, to further obtain nutrition from plants and promote reproduction (Jones & Dangl, 2006; Kamoun, 2006). For example, *Fusarium*

oxysporum secretes multiple effectors suppressing the flg22-triggered reactive oxygen species (ROS) burst in *Nicotiana benthamiana* (Tintor *et al.*, 2020). Another conserved fungal effector protein, NIS1, specifically reduces the kinase activity of BIK1, thereby inhibiting the PAMP-induced ROS burst (Irieda *et al.*, 2019). Pathogens also employ countermeasures against the ETI immune response. The effectors AvrPtoBM3 and HopI1 from *Pseudomonas syringae* DC3000 inhibit cell death induced by HopAD1 and HopQ1-1, respectively (Wei *et al.*, 2018). HopAM1 inhibits immune signaling by mimicking the enzymatic activity of TIR-NLRs in the plant immune system (Eastman *et al.*, 2022). PTI and ETI share some common features, including the production and accumulation of ROS (Tsuda & Katagiri, 2010). However, the accrual of excessive ROS is also toxic to cells, and plants need to maintain a balanced redox homeostasis through modulation of the balance between ROS production and scavenging (Nanda *et al.*, 2010; Tripathy & Oelmüller, 2012; Noctor *et al.*, 2016).

*These authors contributed equally to this work.

Plants have evolved multiple antioxidant mechanisms to scavenge ROS, including small-molecule non-enzymatic antioxidants and enzymatic scavenging systems such as superoxide dismutase (SOD), catalase (CAT), glutathione peroxidase (GPX), and ascorbate peroxidase (APX) (Balaban *et al.*, 2005). APX is a primary enzyme involved in ROS scavenging in various organelles of plants, including the cytoplasm, chloroplasts, mitochondria, and peroxisomes (Diaz-Vivancos *et al.*, 2006; Li, 2023). Its activity was manifested using ascorbic acid as a donor to catalyze the reduction in H₂O₂ to water (Raven, 2000). To date, investigations in plant peroxisome-localized APX have predominantly focused on physiological, biochemical, and abiotic stresses. Overexpression of *AzAPX3* in tobacco protected leaves from aminotriazole-induced oxidative stress damage (Wang *et al.*, 1999). Both APX3 and APX4 in rice are localized in the peroxisome, and their co-silencing could cause early leaf senescence but not growth differences (Ribeiro *et al.*, 2017). Rice CAT deficiency causes high photorespiratory H₂O₂, and knocking out the peroxisome APX triggers an antioxidant mechanism with a compensatory effect on CAT deficiency (Sousa *et al.*, 2015). Outside the important functions outlined previously, APX also plays a role in plant resistance to pathogens. For example, stable expression of an ascorbate peroxidase-like 1 gene, *CAPOA1*, from pepper, enhanced tobacco resistance to *Phytophthora parasitica* (Sarowar *et al.*, 2005). Overexpressing lines of thylakoid membrane-bound ascorbate peroxidase OsAPX8 showed increased resistance to bacterial blight, in which H₂O₂ accumulation was substantially lower than wild-type (WT) and RNAi plants (Jiang *et al.*, 2016). Overexpression of *ZmAPX1* in maize increased tolerance to *Bipolaris maydis* partially due to decreased H₂O₂ accumulation (Zhang *et al.*, 2022). However, the underlying function of peroxisome-localized APX in resistance to disease remained poorly understood.

In the past 15 yr, several investigations have focused on understanding how pathogenic effectors inhibit plant immunity. It was reported that certain effectors of pathogens could specifically target proteins associated with ROS scavenging, causing the suppression of plant immunity. For instance, two CRN effectors from *Phytophthora sojae*, PsCRN63 and PsCRN115, sharing almost identical amino acid sequences, but PsCRN63 induces programmed cell death (PCD) while PsCRN115 inhibits it in plant (Liu *et al.*, 2011). Further research revealed that PsCRN63 and PsCRN115 can manipulate plant PCD by interfering with CAT1 and perturbing H₂O₂ homeostasis (Zhang *et al.*, 2015). RESISTANCE OF RICE TO DISEASES1 (ROD1), a Ca²⁺ sensor, was determined to activate ROS scavenging by interacting with catalase (CatB) to suppress rice immunity. This mechanism was exploited by the fungal effector AvrPiz-t, to promote pathogen virulence (Gao *et al.*, 2021). Various ROS-scavenging-related proteins have been characterized in plants; however, knowledge about pathogen effectors disturbing the function of other ROS-scavenging-related proteins to promote infection remains limited.

In this study, we identified a conserved RXLR effector PpE18, which was required for the full pathogenicity of *P. parasitica* and suppressed plant immunity. We found that PpE18 interacted with an ascorbate peroxidase, NbAPX3-1, which also interacted with ankyrin repeat-containing protein NbANKr2. Moreover, PpE18

inhibited plant immunity by restraining the catalytic activity of NbAPX3-1 and interfering with the association between NbAPX3-1 and NbANKr2. In conclusion, this research documented a mechanism by which *P. parasitica* attacks the host plant to promote infection, deepening our understanding of plant–pathogen interactions.

Materials and Methods

Growth conditions for plants and microorganisms

Nicotiana benthamiana seeds were planted in plastic pots containing a mixture of substrate soil and vermiculite at a ratio of 2 : 1 (v/v). The pots were then placed in a controlled growth chamber with 13 h : 11 h, light : dark circadian rhythm at 23°C. For *Arabidopsis thaliana* (L.) Heynhold, sterile seedlings were planted in soil as previously described (Wang *et al.*, 2011; Li *et al.*, 2020). *Phytophthora parasitica* Dastur strain Pp016 was used in this study. It was cultured as described previously (Wang *et al.*, 2011; Huang *et al.*, 2019). *Escherichia coli* strains DH5 α and BL21 were cultured on Luria–Bertani medium at 37°C with appropriate antibiotics. *Agrobacterium tumefaciens* strain GV3101 was cultured on LB medium at 28°C with appropriate antibiotics.

Stable transformation of *A. thaliana* and *P. parasitica*

To obtain stable transgenic lines of PpE18 in *A. thaliana*, GFP-PpE18 was transformed into *A. thaliana* WT Col-0 using the floral dipping method (Clough & Bent, 1998). To acquire PpE18 knockout transformants, PpE18 was knocked out using CRISPR/Cas9 technology in the Pp016 strain, as previously described (Zhang *et al.*, 2020).

Plasmid construction

PpE18 (lacking signal peptide) was amplified from the *P. parasitica* strain Pp016 cDNA using gene-specific primers, and full-length *NbAPX3-1* and *NbANKr2* were amplified from *N. benthamiana* cDNA using gene-specific primers with FastPfu DNA polymerase (Cat no. AP221; Transgene Biotech, Beijing, China). For overexpression vectors, coding sequences were inserted between the *Xho*I (Cat no. R0146V; New England Biolabs (NEB), Ipswich, MA, USA) and *Xba*I (Cat no. R0145V; NEB) sites of pART27-pro35S-Flag vector (Zhang *et al.*, 2020) or cloned between the *Xho*I and *Hind*III (Cat no. R3104V; NEB) sites of pART27-pro35S-4Myc vector (Fan *et al.*, 2018). To prepare the GFP fusion gene, we inserted GFP into the binary vector PAPK (Gou *et al.*, 2022), introducing multiple cleavage sites before the C-terminal stop codon of GFP, named pART27-pro35S-GFP, as an intermediate vector for simple expression of GFP. To fuse the GFP-tag to the N-terminal of the gene, the coding sequences were inserted between the *Eco*RI (Cat no. R3101V; NEB) and *Xba*I sites of pART27-pro35S-GFP. To integrate the GFP-tag to the C-terminal of the gene, the coding sequence was cloned into the *Xho*I site of pART27-pro35S-GFP.

To create luciferase complementary vectors, the coding region of the target gene was inserted between the *Kpn*I (Cat no. R3142V;

NEB) and *SalI* (Cat no. R3138V, NEB) sites of pCAMBIA1300-nLuc or pCAMBIA1300-cLuc vector. For tobacco rattle virus (TRV)-based virus-induced gene silencing (VIGS) of *NbAPX3-1* or *NbANKr2* in *N. benthamiana*, c. 200–300 bp specific fragment of each gene was selected via the VIGS tool (<https://vigs.solgenomics.net/>) and amplified from *N. benthamiana* cDNA. The PCR products were inserted into pTRV2 vector between the *XbaI* and *BamHI* (Cat no. R3136V; NEB) sites.

To generate constructs of prokaryotic expression assay, the coding sequence of *PpE18*, *NbAPX3-1*, and *NbAPX3-1^{H89A}* was inserted into PET32a at the *NcoI* (Cat no. R3193V; NEB) and *XhoI* sites to construct His-tagged recombinant plasmids. Alternatively, insertion of the *NbAPX3-1* and *NbANKr2* fragments into the pEGX-6P-1 vector at the *BamHI* and *XhoI* sites to construct the GST-tag recombinant plasmids. The CRISPR/Cas9 constructs were conducted as previously described (Zhang *et al.*, 2020). The redox-sensitive GFP (Waypa *et al.*, 2010) fused with SKL (roGFP2-SKL) was inserted into the PAPK vector at the *XhoI* and *XbaI* sites. All primers we used are listed in Supporting Information Table S1.

Reverse transcription-quantitative PCR analysis

Total RNA of *N. benthamiana* leaves, *Arabidopsis* leaves or Pp016 mycelium was extracted using RNA extraction kit (Cat no. DP419; Tiangen, Beijing, China). RNA was reversely transcribed to cDNA using PrimeScript RT reagent Kit (Cat no. AG11728; Accurate Biology, Changsha, China). Real-time quantitative polymerase chain reaction (qPCR) was performed in 20 μ l reaction volume using 10 μ l UltraSYBR Mixture (Cat no. CW0957H; CWBIO, Beijing, China) and 5 μ l cDNA (10 times diluted). The relative expression level of the target gene was calculated using the comparative $2^{-\Delta\Delta Ct}$ method with the internal reference gene *WS041* (Zhang *et al.*, 2012) for *P. parasitica* and *NbEF1 α* (Zhang *et al.*, 2015) for *N. benthamiana*. The primers used in this assay are listed in Table S1.

Transient expression and VIGS in *N. benthamiana*

For *A. tumefaciens*-mediated transient expression assays in *N. benthamiana*, bacterial cells were resuspended and diluted as previously described (Huang *et al.*, 2019; Gou *et al.*, 2022). Resuspended bacteria were infiltrated into the abaxial side of 4- to 5-wk-old *N. benthamiana* leaves with a final optical density OD₆₀₀ of 0.3–1.2. For VIGS assays, *A. tumefaciens* strain carrying vector pTRV1 was co-infiltrated with bacteria harboring different pTRV2 constructs at a final concentration of OD₆₀₀ value of 0.3. pTRV2-GFP or pTRV2-GUS as a control and pTRV2-PDS was used to indicate silencing (Liu *et al.*, 2002a). As previously reported, the two largest leaves of four-leaf-stage seedlings were used for VIGS infiltration (Ratcliff *et al.*, 2001; Liu *et al.*, 2002b). Two to three weeks later, the leaves were used for further analyses.

P. parasitica infection assays

Root infection of *Arabidopsis* sterile seedlings was performed as previously reported (Li *et al.*, 2020), and infection assays on

N. benthamiana leaves were conducted as previously described (Zhang *et al.*, 2020).

Microscopy

Nicotiana benthamiana leaves co-expressing GFP and mCherry-tagged proteins were observed 3 d after infiltration using an Olympus FV3000 confocal microscope (Olympus, Tokyo, Japan). Peroxisomal ROS measurement was conducted as previously described, with minor modifications (Meyer *et al.*, 2007; Yang *et al.*, 2017). *Nicotiana benthamiana* leaves co-expressing roGFP2-SKL and EV, *NbAPX3-1*, *PpE18* or *PpE18* + *NbAPX3-1* were observed using Olympus FV3000 confocal microscope 3 d after infiltration. roGFP2-SKL was excited with 405 and 488 nm lasers, and the emission spectra were collected at 505–545 nm. Fluorescent intensities were examined using IMAGEJ (Schneider *et al.*, 2012) by determining the integral gray value, and the fluorescence intensity ratio of 405 : 488 nm was calculated.

Recombinant protein expression and purification

The recombinant plasmids His-NbAPX3-1, His-NbANKr2, His-NbAPX3-1^{H89A}, GST-NbAPX3-1, GST-NbANKr2, and empty vector only containing His-tag or GST-tag were transformed into *E. coli* strain BL21 cells for protein expression at 37°C. And then induced with IPTG (1 mM final concentration) overnight at 18°C. The induced cells were lysed via sonication. The supernatant was centrifuged at 6000 *g* for 10 min and harvested at 4°C, and the recombinant proteins with His-tag were purified using Ni NTA 6FF beads (Cat#SA005005; Smart-Lifesciences, Changzhou, China). The recombinant proteins with GST-tag were purified using glutathione beads 4FF (Cat#SA010005; Smart-Lifesciences).

His-PpE18 is an insoluble protein in inclusion bodies. The protocol for purification of inclusion body protein followed manufacturer (BioRun Biotechnology, Wuhan, China) protocol, with minor modifications. Specifically, the induced cells were lysed by sonication and centrifuged at 6000 *g* for 10 min to collect the precipitated fraction, which was solubilized with dissolution buffer (50 mM Tris-HCl, pH 8.0, 150 mM NaCl, and 8 M urea). The solubilized protein was purified using Ni NTA 6FF beads. The initially extracted purified protein was dialyzed and renatured via a 50-fold volume of renaturation buffer (50 mM Tris, pH 8.0, 150 mM NaCl, 4 mM reduced glutathione, 0.4 mM oxidized glutathione, and 6 M / 4 M / 2 M / 1 M / 0.1 M urea) and stirred at 4°C for 12 h. The recombinant protein was concentrated by ultrafiltration. After purification, the recombinant proteins were determined by 10% SDS-PAGE followed by Coomassie blue staining and immunoblotting.

Oxidative burst assay and DAB staining

ROS production was examined using a previously described luminol-based assay (Sang & Macho, 2017). Two-week-silenced *N. benthamiana* leaves were sectioned into 5-mm leaf disks and incubated in water within a culture dish overnight. Then, flg22 (Cat no. CP7201; WSHT, Shanghai, China) at 1 μ M final

concentration was added to 200 μ l of luminescence detection buffer containing luminol and peroxidase. The luminescence was detected for 20–30 min.

3,3'-Diaminobenzidine (DAB) staining was performed using a previously described protocol (Daudi & O'Brien, 2012). Specifically, *N. benthamiana* leaves were collected at 20 to 24 h post inoculation (hpi) and stained with 1 mg ml⁻¹ DAB solution (pH 3.0) for 6 h in the dark at room temperature. Leaves were immersed in the eluent solution of ethanol:acetic acid:glycerol (3 : 1 : 1, v/v/v) and boiled continuously for 15 min. To quantify the results of DAB staining, images were converted to an 8-bit gray-scale format and then inverted. The integral gray value of each disease spot was defined using the IMAGEJ software.

Ascorbate peroxidase activity assay

The ascorbate peroxidase activity of proteins expressed *in vivo* and *in vitro* was conducted as previously published, with minor modifications, by detecting the ascorbate oxidation (Nakano & Asada, 1981). *In vitro*, 1 μ M of recombinant protein was mixed with a reaction buffer (0.5 mM ascorbic acid (AsA), 50 mM potassium phosphate buffer (pH 7.0)), to a total volume of 1 ml. The mixture was moved to a quartz cuvette, and H₂O₂ (1 mM final concentration) was added to start the reaction. The peroxidase activity of the purified NbAPX3-1 or NbAPX3-1^{H89A} proteins was recorded by examining the reduction in absorbance at 290 nm using a UV spectrophotometer (UV2600A; UNIC, Shanghai, China). To analyze the effect of PpE18 on the peroxidase activity of NbAPX3-1, we mixed 1 mM of recombinant protein PpE18 with 1 mM of recombinant protein NbAPX3-1 while incubating for 2.5 h at room temperature. NbAPX3-1 activity was then analyzed as described previously.

In vivo, *N. benthamiana* leaves (300 mg fresh weight) expressing target proteins were harvested 3 d after agroinfiltration. Samples were frozen in liquid nitrogen, grinded, and mixed with 900 μ l of extraction buffer containing 50 mM phosphate buffer (pH 7.0), 1 mM AsA, and 1 mM ethylenediamine tetraacetic acid (EDTA). After centrifugation at 4°C, 100 μ l of supernatant was added to the reaction buffer described previously to a total volume of 1 ml. Samples were analyzed as described previously.

Luciferase complementation assay

Luciferase complementation assays were conducted as previously described (Zhou *et al.*, 2018). *Agrobacterium tumefaciens* GV3101 cells containing the desired plasmids were infiltrated into 5-wk-old *N. benthamiana* leaves, and images were obtained 2 d after infiltration with a low-light cooled CCD camera (PlantView100; BLT, Guangzhou, China). The fluorescence intensity was quantified using the PLANTVIEW100 software.

Co-immunoprecipitation and western blotting

The infiltrated leaves of *N. benthamiana* were harvested, and proteins were extracted using an extraction buffer containing 1% TritonX-100, 50 mM Tris-HCl, pH 7.4, 1% sodium

deoxycholate, 0.1% SDS, 5 mM sodium fluoride, 1 mM sodium orthovanadate, 1 mM EDTA-2Na, 2% PVPP, 150 mM NaCl, 1 mM DTT, 1 \times protease inhibitor, and 1 mM PMSF.

Co-immunoprecipitation assay was performed according to the manufacturers' instructions. Anti-GFP (Cat no. KTSM1334; KT Health, Shenzhen, China), anti-Flag (Cat no. KTSM1338; KT Health), or anti-Myc magarose beads (Cat no. KTSM1336; KT Health) were added to the supernatant and incubated at 4°C for 1–3 h. The precipitates were washed five times with wash buffer. Crude proteins (Input) and immune precipitated proteins were separated by 10% SDS-PAGE gels (Cat no. PG212; Epizyme, Shanghai, China) and detected by immunoblotting as previously described (Fan *et al.*, 2018). Antibodies used for immunoblot assays include mouse anti-DDDDK-Tag (Cat no. AE005; ABclonal, Wuhan, China), mouse anti-GFP-Tag (Cat no. AE012; ABclonal), mouse anti-Myc-Tag (Cat no. AE010; ABclonal), rabbit anti-Luciferase (Cat no. L0159; Sigma), mouse anti-cLuc (Cat no. L2164; Sigma), horseradish peroxidase goat anti-mouse immunoglobulin G (IgG) (Cat#AS003; ABclonal), and goat anti-rabbit IgG (Cat no. AS014; ABclonal).

GST pull-down assays

The pull-down assays were performed according to the manufacturers' instructions of glutathione magarose beads (Smart-Lifesciences). The bound proteins were separated by 10% SDS-PAGE and detected using immunoblotting. Antibodies used for immunoblot assays were as follows: mouse anti-GST-tag mAb (Cat no. AE001; ABclonal), rabbit anti-His-Tag mAb (Cat no. AE086; ABclonal), horseradish peroxidase goat anti-mouse immunoglobulin G (IgG), and goat anti-rabbit IgG.

Statistical analysis

Statistical analysis was performed using Student's *t*-test. Significance was defined at $P < 0.05$. Phylogenetic analysis was performed in the MEGAX64 software using neighbor-joining method with bootstrap values of 1000 (Kumar *et al.*, 2018). Multiple sequence alignment was conducted using CLUSTALW (<https://www.genome.jp/tools-bin/clustalw>) and visualized with JALVIEW (Clamp *et al.*, 2004). Schematic diagram of PpE18 was generated with Adobe Illustrator. The schematic diagram of NbANKr2 was generated using the Prosite program (<https://prosite.expasy.org/mydomains/>). The model for the PpE18 function was drawn by Figdraw (www.figdraw.com, ID: RUPWScfba).

Results

The conserved RXLR effector PpE18 of *Phytophthora parasitica* is a virulence factor

It is well-documented that the RXLR effector genes of oomycetes are typically virulence factors (Wang *et al.*, 2019; Dong & Ma, 2021). To understand *P. parasitica* pathogenesis, RNA-sequencing (RNA-seq) was performed (Jia *et al.*, 2017) to identify highly up-regulated RXLR effector genes in the early stages

of infection. This resulted in the identification of *PpE18*, which was highly expressed during infection (Fig. S1a). The time-course expression profile of *PpE18* during plant infection was confirmed using reverse transcription-quantitative polymerase chain reaction (RT-qPCR) (Bustin *et al.*, 2009), with results consistently demonstrating high levels of expression during early stages of *P. parasitica* infection, peaking at 6 hpi (Fig. S1b). Multiple sequence alignment revealed limited variations in 17 *P. parasitica* strains (Table S2) across different geographic and host plant origins (Fig. S2). These findings suggested that *PpE18* encodes a conserved effector potentially contributing to *P. parasitica* infection.

To evaluate the contribution of *PpE18* to the virulence of *P. parasitica*, we performed CRISPR/Cas9-based knockout experiments in the *P. parasitica* strain Pp016. We successfully obtained two knockout mutants (*PpE18-ko-2* and *PpE18-ko-2A*), as verified using PCR amplification and sequencing of PCR products (Fig. S3a). The mutants exhibited normal mycelial growth rate and colonial morphology, similar to the WT (Fig. S3b,c). Pathogenicity assay on *N. benthamiana* leaves showed significantly reduced virulence, as indicated by smaller lesions compared with the WT Pp016 (Fig. 1a,b).

To further assess its virulence role, we designed *GFP-PpE18* fusion construct and transiently expressed it in *N. benthamiana* leaves via agroinfiltration assay, with *GFP* as a negative control. Two days after infiltration, the agroinfiltrated leaves were inoculated with mycelial plugs of *P. parasitica* Pp016. The results showed that compared with *GFP*, the leaf sides expressing *GFP-PpE18* exhibited significantly larger lesions, indicating that *PpE18* promotes plant susceptibility to *P. parasitica* infection (Fig. 1c,d). The expression and integrity of GFP-PpE18 and GFP proteins were confirmed by western blot (Fig. S4a). We further generated transgenic *A. thaliana* plants stably expressing *PpE18*. Two confirmed *PpE18*-overexpressing transformants (*PpE18-L2* and *PpE18-L10*) were selected for further analyses (Fig. S4b). The 2-wk-old transgenic seedlings were inoculated with *P. parasitica* zoospores. Compared with the control *Flag-GFP*-expressing seedlings, *PpE18*-expressing transformants exhibited a higher disease degrees 2 wk after inoculation (Fig. 1e, f), indicating that *PpE18* overexpressing lines show enhanced susceptibility to *P. parasitica*. Collectively, these results suggested that PpE18 is required for *P. parasitica* virulence.

To analyze the virulence function of PpE18, we determined its subcellular localization in plant cells by transiently expressing *GFP-PpE18* in *N. benthamiana* leaves. The result showed that GFP-PpE18 fluorescence signals overlapped with the peroxisome marker PTS2-mCherry (Lin *et al.*, 2004) and the endoplasmic reticulum (ER) marker mCherry-ER (Fan *et al.*, 2018) (Fig. 1g), indicating that PpE18 is localized on both the peroxisome membrane and ER. The expression and integrity of GFP-PpE18 and marker proteins were confirmed by western blot (Fig. S5a).

PpE18 interacts with NbAPX3-1 in *N. benthamiana*

To explore the virulence mechanism of PpE18, we performed an immunoprecipitation-mass spectrometry (IP-MS) assay in

N. benthamiana to identify its target proteins. Based on the IP-MS data, 48 candidate *N. benthamiana* proteins (Table S3) were selected, and GFP fusion constructs were created. The fusion constructs were transiently co-expressed with the mCherry-tagged PpE18 protein (mCherry-PpE18) construct in *N. benthamiana* to examine their co-localizations. The results showed that the ascorbate peroxidase protein, NbAPX3-1, closely related to AtAPX3 (Fig. S6), co-localized with PpE18 in peroxisome membrane and ER (Fig. 2a), and therefore was selected for further analyses. Western blot indicated that GFP-NbAPX3-1 and mCherry-PpE18 were both successfully expressed (Fig. S5b).

To confirm the interaction between PpE18 and NbAPX3-1, we performed a luciferase complementation assay. Co-expression of *PpE18-nLuc* (N-terminal of luciferase) and *cLuc* (C-terminal of luciferase)-*NbAPX3-1* in *N. benthamiana* leaves via agroinfiltration exhibited a strong catalytic activity of luciferase in the infiltrated area (Fig. S7). Next, the Co-IP assays also confirmed their interaction, with results clearly showing that NbAPX3-1 was enriched by PpE18 instead of the GFP control (Fig. 2b), and PpE18 but not GFP was enriched by NbAPX3-1 (Fig. 2c). Moreover, we purified both GST-NbAPX3-1 and His-PpE18 to performed GST pull-down assay. Our findings demonstrated that GST-NbAPX3-1 could pull down His-PpE18, indicating a direct interaction between PpE18 and NbAPX3-1 (Fig. 2d). Furthermore, we generated five mutants of PpE18 based on the amino acid variations identified in the conservative analysis of PpE18. These mutants retained capacity to interact with NbAPX3-1 in the Co-IP assay (Fig. S8), suggesting that the point mutations do not impact the binding capacity of PpE18 to NbAPX3-1.

The peroxisome membrane localization of NbAPX3-1 is required for its immune function

To investigate the role of *NbAPX3-1* in plant immunity, we silenced it in *N. benthamiana* by VIGS. Quantitative reverse transcription polymerase chain reaction analysis showed that the transcriptional level of *NbAPX3-1* was dramatically reduced compared with the TRV-*GFP* control (Fig. 3a). Infection assay with *P. parasitica* showed that the detached leaves of TRV-*NbAPX3-1* developed larger lesion areas, compared with the control TRV-*GFP* leaves (Fig. 3b,c). Moreover, we transiently expressed *GFP-NbAPX3-1* (left) and control *Flag-GFP* (right) in the *N. benthamiana* leaves, and *P. parasitica* inoculation assay was performed after 3 d. Compared with the control, overexpression of *GFP-NbAPX3-1* resulted in significantly smaller lesions (Fig. 3d, e, left). These results suggested that NbAPX3-1 contributes to plant resistance against *P. parasitica*.

Peroxisome membrane-bound ascorbate peroxidase has a membrane peroxisome-targeting signal (mPTS) at its C-terminal, consisting of a transmembrane domain as well as several amino acid residues (Mullen & Trelease, 2000, 2006). NbAPX3-1 has one mPTS at its C-terminal (Fig. S9), and the transmembrane domain was identified using TMHMM tool (<https://services.healthtech.dtu.dk/services/TMHMM-2.0/>). To characterize the immune role of mPTS in NbAPX3-1, we constructed two NbAPX3-1 truncated

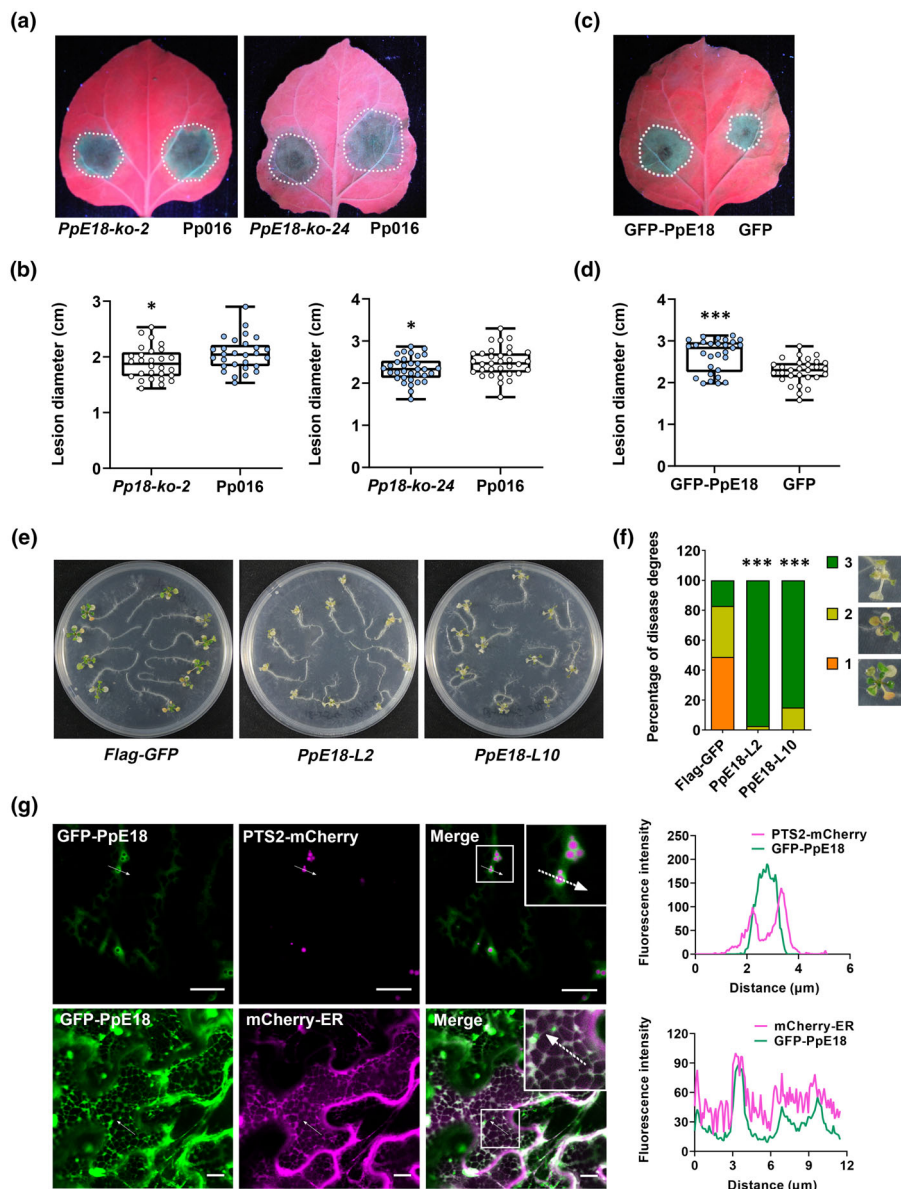


Fig. 1 *PpE18* is a virulence factor of *Phytophthora parasitica*. (a, b) Lesions development of *PpE18-ko-2* and *PpE18-ko-24* on *Nicotiana benthamiana* leaves. The lesion expansion was visualized under UV light (a), and the lesion diameters were measured at 40 h post inoculation, with data (*PpE18-ko-2*, $n = 28$ and *PpE18-ko-24*, $n = 33$) analyzed from three independent experiments (b). Statistical analysis based on Student's *t*-test. Upper quartile, median, and lower quartile values are indicated in each box plot, while the bars outside the box indicate the maximum and minimum values. Asterisks above the bar indicate significant differences: *, $P < 0.05$. (c, d) Transient expression of *PpE18* in *N. benthamiana* leaves followed by *P. parasitica* infection. The lesion expansion was visualized under UV light (c). The lesion diameters were measured from three independent experiments ($n = 39$) at 48 h post inoculation (hpi) (d). Statistical analysis based on Student's *t*-test. Upper quartile, median, and lower quartile values are denoted in each box plot, while the bars outside the box indicate the maximum and minimum values. Asterisks above the bars indicate significant differences: ***, $P < 0.001$. (e, f) Phenotype of root infection in *Arabidopsis* lines expressing *PpE18* and *Flag-GFP*. Two-week-old *Arabidopsis thaliana* sterile seedlings roots were inoculated with *P. parasitica* zoospores. Disease progression was monitored, and images were taken 2 wk after inoculation (e), followed by calculating the disease severity (f). Approximately 40 seedlings of each transformant from two independent experiments were used for analysis. Disease severity was divided into three grades. (1) few leaves turn yellow or die; (2) most of leaves die, but the seedling survives; and (3) seedling dead. Statistical analysis based on Wilcoxon rank sum test (***, $P < 0.001$). (g) Subcellular localization of *PpE18* in *N. benthamiana*. *GFP-PpE18* was co-expressed with *PTS2-mCherry* or *mCherry-ER* in *N. benthamiana* leaves. Fluorescence plots show the fluorescence intensities along the arrows indicated on the images. Bars, 10 μm . *PTS2-mCherry* is a peroxisome marker and *mCherry-ER* is an endoplasmic reticulum marker.

mutants based on whether mPTS were deleted or not, namely NbAPX3-1-mPTS (only mPTS is retained, the rest is all truncated) and NbAPX3-1 ΔmPTS , and determined their subcellular

localization in *N. benthamiana* leaves. The results showed that NbAPX3-1 was localized both on the peroxisome membrane and ER (Fig. S10a,c). NbAPX3-1-mPTS had obvious peroxisome

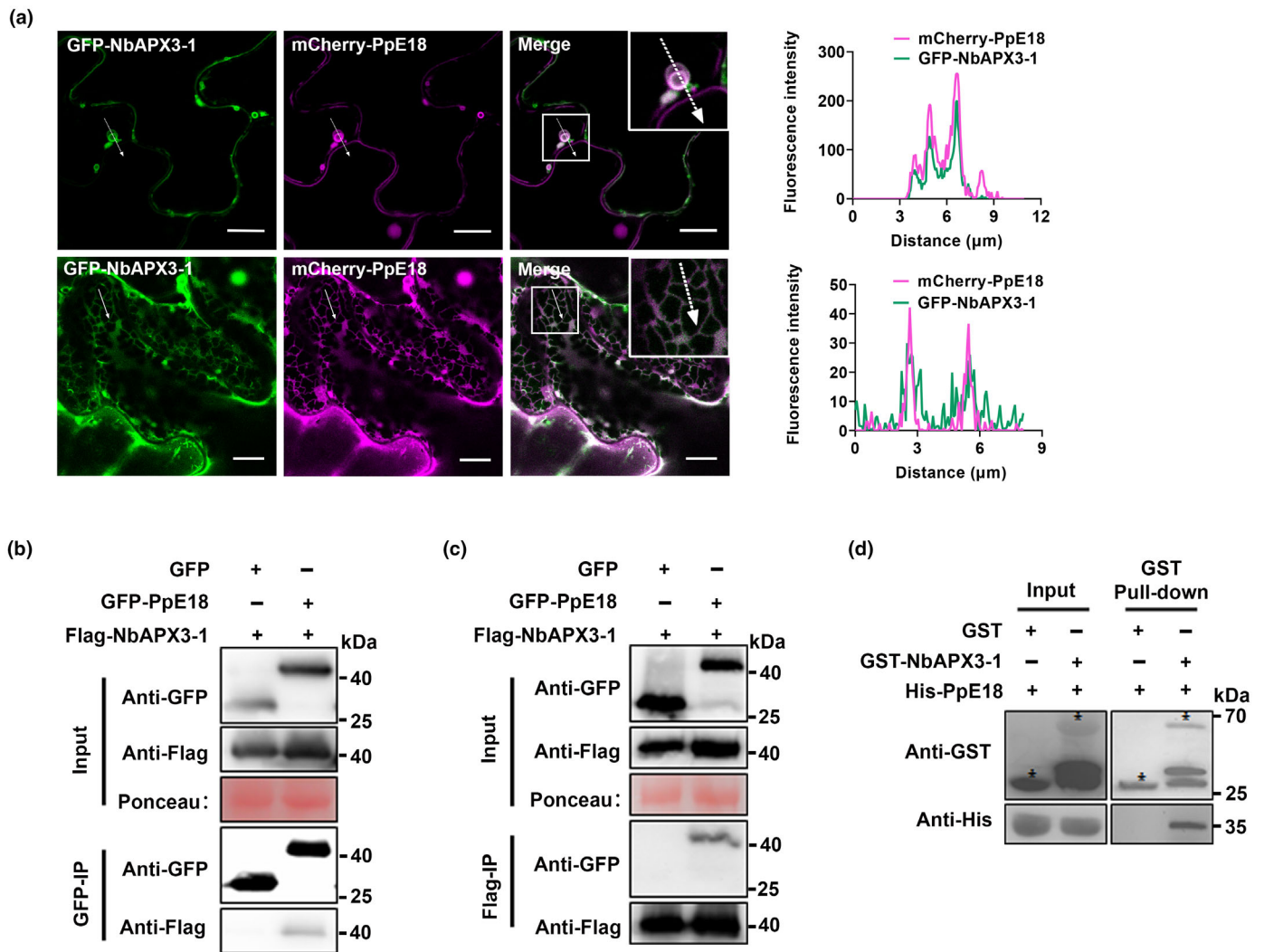
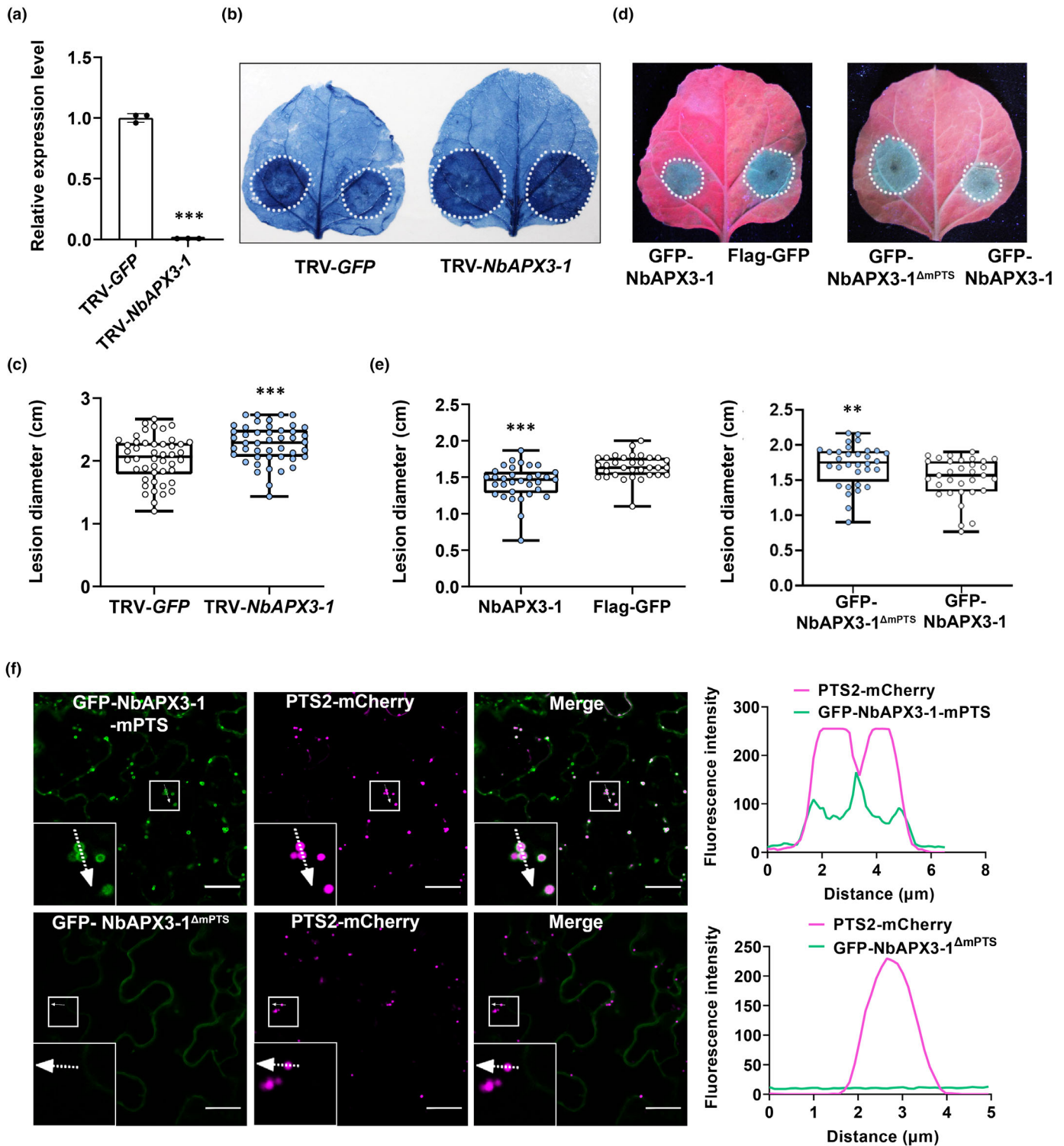


Fig. 2 PpE18 physically interacts with NbAPX3-1 on the peroxisome membrane and endoplasmic reticulum. (a) Subcellular localization of PpE18 and NbAPX3-1. The upper and lower panel images indicate peroxisome membrane localization and endoplasmic reticulum localization, respectively. Fluorescence plots show the fluorescence intensities along the arrows indicated on the images. Bars, 10 μm . (b, c) Co-immunoprecipitation shows interaction between GFP-PpE18 and Flag-NbAPX3-1. Total proteins were extracted from *Nicotiana benthamiana* leaves expressing the indicated proteins. The interaction complexes were immunoprecipitated with GFP- or Flag-Trap beads, and immunoblotting was performed using anti-GFP and anti-Flag antibodies. Similar results were observed in three independent experiments. (d) GST pull-down assay shows interaction between His-PpE18 and GST-NbAPX3-1. His-PpE18, GST-NbAPX3-1 and GST proteins were expressed in *Escherichia coli*. The pull-down inputs and samples were detected by western blot using anti-GST or anti-His antibodies, respectively. Asterisks indicate the objective bands. The experiment was performed two times with similar results.

Fig. 3 Peroxisome membrane localization was critical for the positive immune function of NbAPX3-1 to *Phytophthora parasitica*. (a–c) *Phytophthora parasitica* inoculation assay on TRV-GFP and TRV-NbAPX3-1 plants. The transcription level of NbAPX3-1 in TRV-NbAPX3-1 and TRV-GFP plants is shown in (a). *NbEF1 α* served as reference gene for transcript normalization. Data are presented as means \pm SD ($n = 3$), asterisk above the error bar indicates significant differences (***, $P < 0.001$; Student's *t*-test). The disease expansion was visualized by trypan blue staining (b). The lesions ($n = 46$) in leaves were measured at 40 h post inoculation (hpi). Data were calculated from three independent experiments (c). (d, e) *Phytophthora parasitica* inoculation assay on leaves overexpressing Flag-GFP, NbAPX3-1, or GFP-NbAPX3-1^{AmPTS}. The disease expansion was visualized under UV light (d). The lesions diameters were measured at 48 hpi, data (left panel, $n = 33$; right panel, $n = 32$) were calculated from three independent experiments (e). Statistical analysis in (c, e) based on Student's *t*-test. Upper quartile, median, and lower quartile values are indicated in each box plot, while the bars outside the box indicate the maximum and minimum values. Asterisks above the bars indicate significant differences: **, $P < 0.01$; ***, $P < 0.001$. (f) Subcellular localization of NbAPX3-1 mutants. GFP-NbAPX3-1^{AmPTS} and GFP-NbAPX3-1^{mPTS} were co-expressed with PTS2-mCherry in *Nicotiana benthamiana* leaves, respectively. Fluorescence plots show the fluorescence intensities along the arrows. Bars, 20 μm . The white box outlines the area shown at higher magnification at the indicated magnification.



membrane localization while NbAPX3-1 Δ mPTS was hardly observed (Figs 3f, S10e), but both were still localized to the ER (Fig. S10b,d). Furthermore, PpE18 interacted mainly with NbAPX3-1-mPTS (Fig. S11), suggesting that the mPTS is crucial for the peroxisome membrane localization of NbAPX3-1, and the interaction between PpE18 and NbAPX3-1 mostly occurs on the

peroxisome membrane. Intriguingly, the disease resistance of NbAPX3-1 Δ mPTS was significantly reduced compared with the control NbAPX3-1 using a *P. parasitica* inoculation assay on GFP-NbAPX3-1 Δ mPTS or GFP-NbAPX3-1 overexpression leaves (Fig. 3d,e, right). Western blot indicated that GFP-NbAPX3-1 Δ mPTS and GFP-NbAPX3-1 were both successfully expressed

(Fig. S12). These results suggested that the mPTS is critical for the regulation of NbAPX3-1 on plant immunity to *P. parasitica*. Taken together, the positive immune regulation of NbAPX3-1 is dependent on its peroxisome membrane localization.

ROS-scavenging activity of NbAPX3-1 is crucial for its immune function

Ascorbate peroxidase is associated with H₂O₂ scavenging (Li, 2023). To further analyze the molecular function of NbAPX3-1, we investigated its ability to scavenge H₂O₂. We found that flg22-induced ROS production was prompted in the *NbAPX3*-silenced leaves, compared with TRV-*GFP* control (Fig. 4a), suggesting that NbAPX3-1 might affect ROS accumulation. We evaluated H₂O₂ accumulation through DAB staining in *NbAPX3-1*-silenced leaves following *P. parasitica* inoculation. The results indicated that *NbAPX3-1*-silenced leaves had much stronger H₂O₂ accumulation than the TRV-*GFP* leaves in the early stage of disease development (Fig. 4b,c). Moreover, because the localization of peroxisome membrane is critical to *NbAPX3-1*, we also measured the redox changes in peroxisomes by the expression of a redox-sensitive fluorescent reporter fused to the peroxisome serine-lysine-leucine (SKL) targeting signal (roGFP2-SKL) (Meyer *et al.*, 2007; Yang *et al.*, 2017) to enable visualization of peroxisomal redox status in *NbAPX3-1*-silenced leaves. roGFP2-SKL with a larger 405 nm/488 nm fluorescence intensity ratio indicated increased oxidative stress. The results showed that silencing *NbAPX3-1* resulted in an increased peroxisomal redox value of 1.961, compared with 0.672 for TRV-*GUS* leaves (Fig. 4e,f), suggesting more ROS accumulated inside peroxisomes in *NbAPX3-1*-silenced leaves. These findings suggested that *NbAPX3-1* negatively regulates H₂O₂ production and accumulation in *N. benthamiana*.

To further verify the regulatory effect of NbAPX3-1 on ROS, we expressed and purified the recombinant NbAPX3-1 in *E. coli* (Fig. S13a) and tested APX enzymatic activity *in vitro*. We observed that the rate of ascorbate depletion was significantly faster in the presence of NbAPX3-1 than in the empty control (Fig. 4d). His42 was found to be one of the key residues in the active site of the soybean cytosolic ascorbate peroxidase GmAPX1 (Sharp *et al.*, 2003). Sequence analyses showed that His89 in NbAPX3-1 corresponded to His42 in GmAPX1 (Fig. S9). To investigate the role of NbAPX3-1 as a typical ascorbate peroxidase, we constructed a mutant NbAPX3-1^{H89A}, in which His89 was replaced with alanine, and performed recombinant protein expression and purification (Fig. S13a). The APX enzymatic activity assay showed that the ascorbate peroxidase activity of mutant NbAPX3-1^{H89A} was decreased significantly compared with the WT NbAPX3-1 *in vitro* (Fig. 4d), indicating that His89 is necessary for APX activity. Ultimately, these results indicated that NbAPX3-1 could scavenge ROS directly.

To examine whether the enzyme activity of NbAPX3-1 is required for its immune function, we transiently expressed *GFP-NbAPX3-1* (right) and *GFP-NbAPX3-1^{H89A}* (left) in *N. benthamiana* leaves via agroinfiltration, followed by *P. parasitica* inoculation. The result showed that the expression of *GFP-*

NbAPX3-1^{H89A} resulted in larger lesion sizes compared with the *GFP-NbAPX3-1* (Fig. 4g-i), indicating that the NbAPX3-1-mediated plant resistance relies on its ROS scavenge function.

PpE18 inhibits the ROS-scavenging function of NbAPX3-1

Influencing the stability and function of plant immune-related proteins through effectors has been documented as an effective strategy for pathogens to interfere with plant immunity (Ai *et al.*, 2021). To examine whether PpE18 affects the stability of NbAPX3-1 during interaction, *GFP-PpE18* or *GFP* was transiently co-expressed with *Flag-NbAPX3-1* in *N. benthamiana* leaves, and NbAPX3-1 protein levels were quantified by immunoblots. As shown in Fig. S14, PpE18 did not affect the accumulation of NbAPX3-1 compared with GFP.

To further explore how PpE18 targets NbAPX3-1 to suppress plant immunity, we analyzed whether the APX catalytic activity of NbAPX3-1 is affected by PpE18 *in vitro*. Expression and purification of recombinant proteins were confirmed by SDS-PAGE analysis (Fig. S13b). His-NbAPX3-1 was incubated with His-PpE18 or negative control EV to analyze the activity of NbAPX3-1. The results showed that in the presence of PpE18, the APX activity of NbAPX3-1 significantly decreased compared with that in the presence of EV (Fig. 5a), suggesting that the PpE18 binding attenuates the enzyme activity of NbAPX3-1. We further performed agroinfiltration to transiently co-express *GFP-PpE18* or *GFP* with *GFP-NbAPX3-1* in *N. benthamiana* leaves to determine whether PpE18 inhibits the activity of NbAPX3-1 *in vivo*. The results indicated that PpE18 does not affect the endogenous APX activity of leaves (Fig. S15a,b), but remarkably reduces the activity of NbAPX3-1 (Fig. 5b). The expression and integrity of GFP, GFP-NbAPX3-1, and GFP-PpE18 proteins were confirmed by western blot (Fig. S16).

Subsequently, we also tested whether PpE18 affects the redox state of peroxisome by inhibiting the activity of NbAPX3-1 through the expression of *roGFP2-SKL*. We found that overexpression of *NbAPX3-1* resulted in a reduced peroxisome redox value of 0.346, compared with 0.983 for leaves overexpression of *EV*, indicating lower ROS level inside peroxisomes during *NbAPX3-1* expression (Fig. 5c,d), possibly resulting from scavenging of ROS by NbAPX3-1. We also found that overexpression of *PpE18* alone had no effect on the redox state of leaves (Fig. S15c,d). However, the co-expression of *PpE18* and *NbAPX3-1* resulted in an increased peroxisomal redox value of 0.944, compared with 0.495 for the co-expression of *EV* and *NbAPX3-1* (Fig. 5c,d), indicating ROS-scavenging function of NbAPX3-1 could be attenuated by PpE18. Taken together, these results indicated that PpE18 can suppress the enzyme activity of NbAPX3-1.

NbANKr2 interacts with and is required for NbAPX3-1-mediated plant immunity

AtAPX3 is stabilized by AtAKR2A (Yan *et al.*, 2002; Shen *et al.*, 2010). We examined whether the stability of NbAPX3-1 could be affected by NbANKr2, a homolog of AtAKR2A

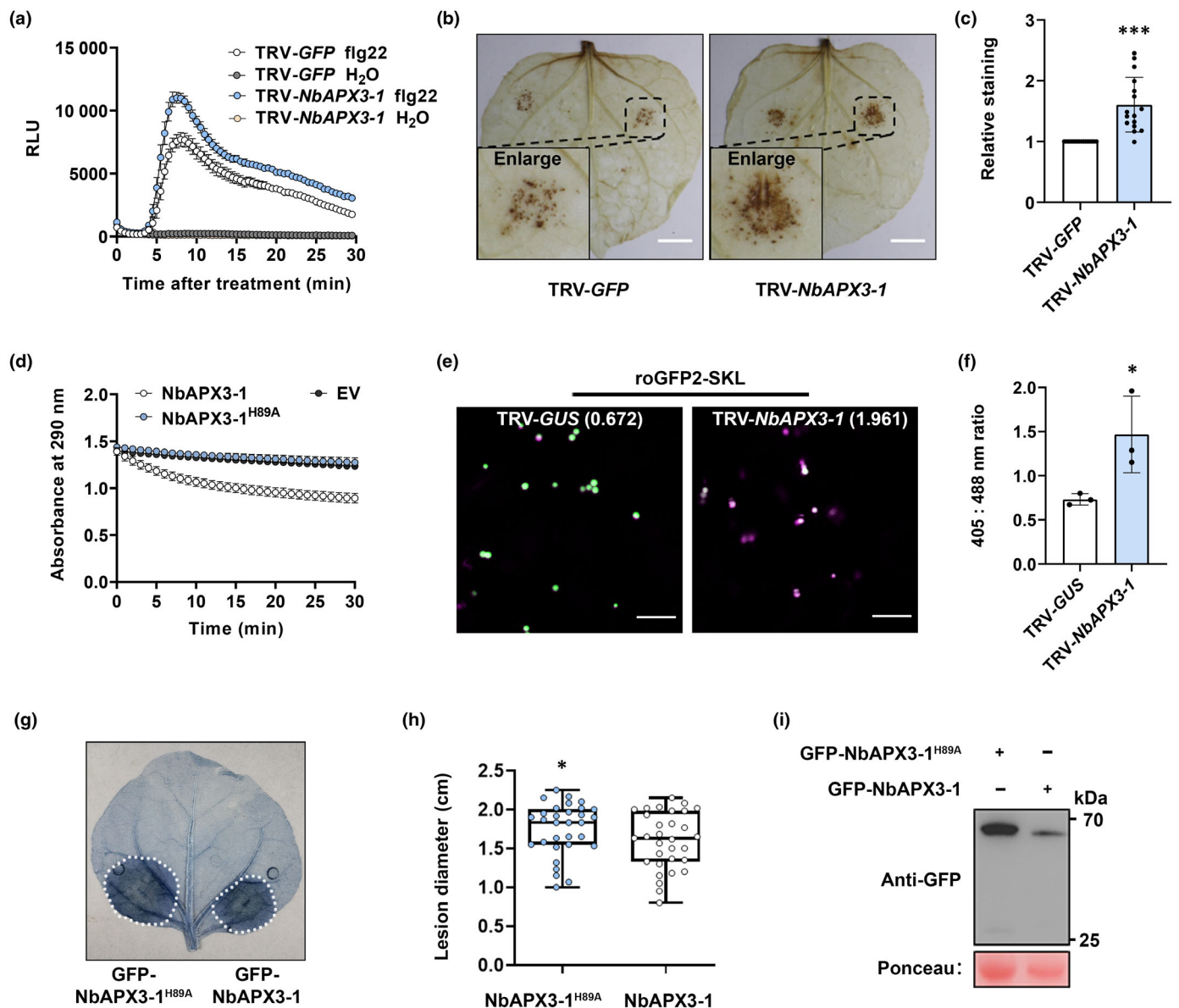


Fig. 4 NbAPX3-1-mediated plant resistance relies on its reactive oxygen species (ROS)-scavenging function. (a) ROS burst excited by flg22 in the TRV-*GFP* and TRV-*NbAPX3-1* plants was analyzed. Relative luminescence units indicated the relative amounts of H₂O₂ production induced by 1 mM flg22 in leaf disks. Each data point consists of 12 replicates. Error bars indicate SE. The experiment was triplicated with similar results. (b, c) H₂O₂ accumulation in TRV-*GFP* and TRV-*NbAPX3-1* leaves challenged with *Phytophthora parasitica*. Leaves were collected for 3,3'-diaminobenzidine (DAB) staining at 24 h post inoculation (hpi) (b). Bars, 10 mm. Integral gray values of the DAB-stained region were analyzed using IMAGEJ (c). DAB staining intensity of TRV-*GFP* leaves were set to 1. Data and error bars were calculated from three independent experiments. Error bars represent mean ± SD (*n* = 16). Asterisk above the error bar indicates significant differences: ***, *P* < 0.001 (Student's *t*-test). (d) Ascorbate peroxidase catalytic activity of NbAPX3-1 and NbAPX3-1^{H89A} *in vitro*. The recombinant proteins His-NbAPX3-1^{H89A}, His-NbAPX3-1, and empty vector were expressed and purified from *Escherichia coli*. Each data point consists of three replicates. Error bars indicate SE. The experiment was performed two times with similar results. (e, f) Peroxisomal redox status of TRV-*GUS* and TRV-*NbAPX3-1* leaves after 3 d agroinfiltration of roGFP2-SKL. Fluorescence excited by 405 and 488 nm laser was collected at 505–545 nm using a confocal microscope. Merged images of 405 and 488 nm channels are shown in (e), and the ratios of 405 : 488 nm are shown in (f). Bars, 10 μm. Three images from each group were used for statistical analysis. Data represent mean ± SD. Asterisk above the error bar indicates significance: *, *P* < 0.05 (Student's *t*-test). Two independent experiments were conducted and yielded similar results. (g–i) *Phytophthora parasitica* infection in leaves expressing GFP-*NbAPX3-1*^{H89A} and GFP-*NbAPX3-1*. The disease expansion was visualized by trypan blue staining (g), and the lesions diameters were measured at 48 hpi. Data (*n* = 31) were calculated from three independent experiments (h). Statistical analysis based on Student's *t*-test. Upper quartile, median, and lower quartile values are indicated in each box plot, while the bars outside the box indicate the maximum and minimum values. Asterisk above the bar indicates significance: *, *P* < 0.05. Western blotting shows the protein level of GFP-*NbAPX3-1*^{H89A} and GFP-*NbAPX3-1* in *Nicotiana benthamiana* leaves using anti-GFP antibody (i).

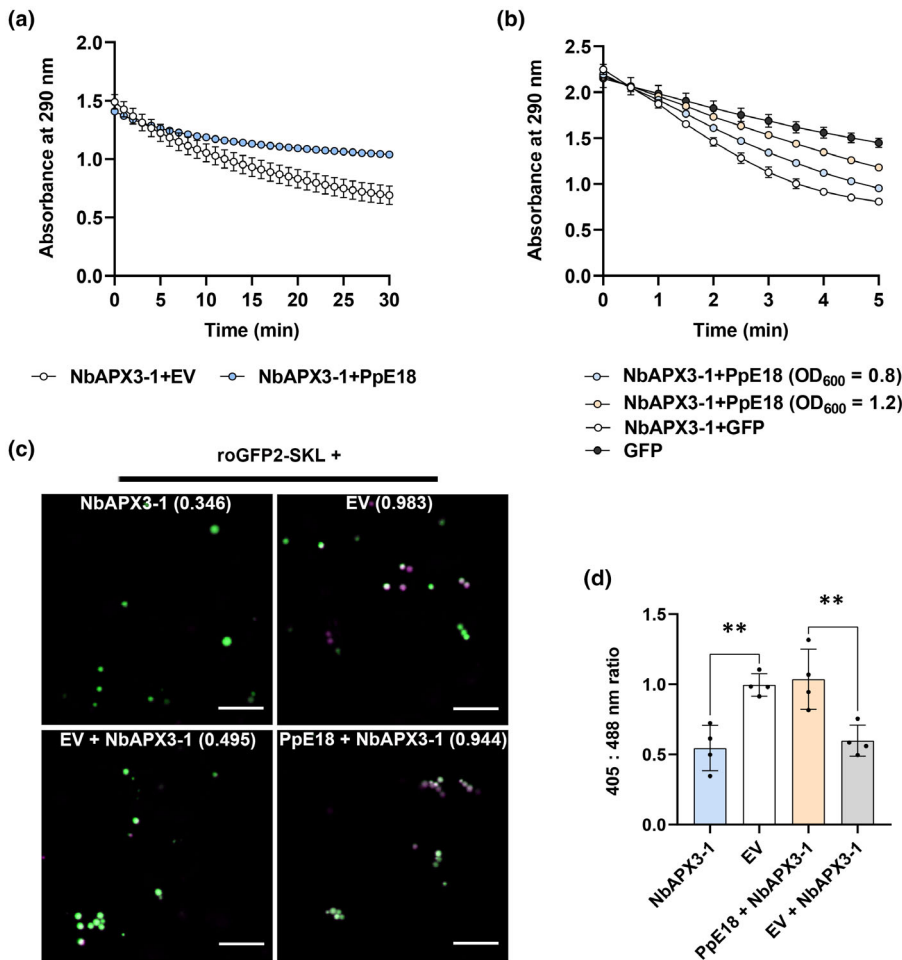


Fig. 5 PpE18 inhibits the function of NbAPX3-1 in reactive oxygen species scavenging. (a) Ascorbate peroxidase (APX) activity assay for NbAPX3-1 in the presence or absence of PpE18 *in vitro*. Recombinant proteins His-NbAPX3-1, His-PpE18, and empty vector (EV) were expressed and purified from *Escherichia coli*. Each data point consists of two replicates. Error bars indicate SE. The experiment was performed three times with similar results. (b) The APX activity of NbAPX3-1 in the presence of different PpE18 concentrations *in vivo*. Proteins were expressed using agroinfiltration method. Each data point consists of three replicates, and error bars indicate SE. The experiment was performed three times with similar results. (c, d) The peroxisomal redox status of leaves that co-expressed NbAPX3-1, EV, PpE18 + NbAPX3-1, or EV + NbAPX3-1 with roGFP2-SKL. Images taken at 405 and 488 nm laser by confocal microscope were merged, and the representative photographs with 405 : 488 nm ratios are shown in (c). Bars, 10 μ m. At least four images from each group were used for statistical analysis (d). Data represent mean \pm SD. Asterisks above the error bars indicate significance: **, $P < 0.01$ (Student's *t*-test). Three independent experiments were conducted and yielded similar results.

(Fig. S17). We confirmed the interaction between NbANKr2 and NbAPX3-1 using a Co-IP assay, when the fusion construct GFP-NbAPX3-1 was co-expressed with Flag-NbANKr2, but not the negative control GFP (Fig. S18a). Their interaction was also confirmed by GST pull-down assay (Fig. S18b).

APX proteins primarily function as dimers (Patterson & Poulos, 1995; Hong *et al.*, 2018; Kaur *et al.*, 2021). Consistently, we detected significant accumulation of NbAPX3-1 dimers using a Co-IP assay (Fig. S19). To understand the molecular mechanism of NbANKr2-NbAPX3-1 interaction, we investigated the effect of NbANKr2 on the dimerization of NbAPX3-1. We conducted a Co-IP assay on Flag-NbAPX3-1 and Myc-NbAPX3-1 in the presence or absence of NbANKr2-GFP. As shown in Fig. 6(a), the protein level of Flag-NbAPX3-1 was increased when co-expressed with both Myc-NbAPX3-1 and NbANKr2-GFP. Moreover, we evaluated the dimerization of NbAPX3-1 in the presence or absence of Flag-NbANKr2 in *N. benthamiana* leaves by using a luciferase complementary assay. We found that the presence of Flag-NbANKr2 significantly improved the degree of dimerization indicated by increased luciferase activity compared with leaf regions infiltrated with Flag-GFP (Fig. 6b,c). Subsequently, we analyzed the influence of NbANKr2 on the protein accumulation of NbAPX3-1 by western blot. We co-expressed

NbANKr2-GFP or negative control GFP with Flag-NbAPX3-1 in *N. benthamiana*. The protein accumulation of NbAPX3-1 was increased at both 2 and 3 d after infiltration (Fig. 6d), indicating that NbANKr2 improves the stability of NbAPX3-1 *in planta*.

To understand whether NbANKr2 influences the NbAPX3-1-mediated disease resistance, we performed VIGS assay in *N. benthamiana*. Given the high sequence similarity between NbANKr1 and the homolog, NbANKr2 (Vaira *et al.*, 2018), we designed the silencing vectors to target the two genes. Quantitative reverse transcription polymerase chain reaction analysis showed that the transcriptional level of NbANKr2 was dramatically reduced compared with the TRV-GUS control (Fig. S20a). Infection assays showed that the NbANKr-silenced plants were more susceptible to *P. parasitica* than GUS-silenced plants (Fig. S20b,c). Consistent with this observation, overexpression of NbANKr2 increased *N. benthamiana* resistance to *P. parasitica* (Fig. S20d-f), indicating that NbANKr2 is a positive plant immunity regulator.

Based on the direct interaction between NbAPX3-1 and NbANKr2, we further used a VIGS assay to examine whether NbAPX3-1-mediated plant immunity requires NbANKr2. The results showed that in the TRV-GUS plants, the overexpression of Flag-NbAPX3-1 significantly improved plant resistance to

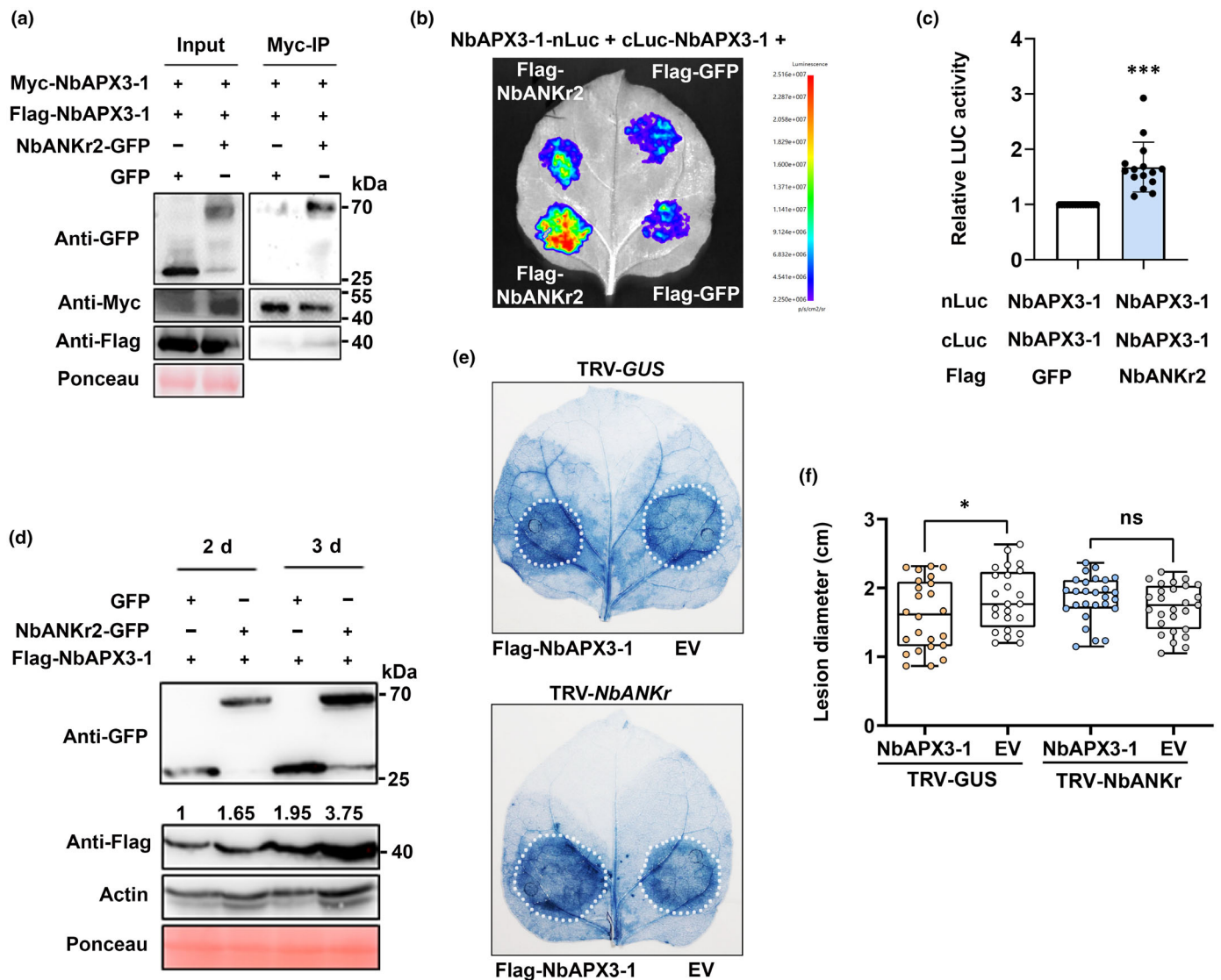


Fig. 6 NbANKr2 is necessary for NbAPX3-1-mediated plant immunity. (a) Co-IP assay shows the effect of NbANKr2 on the dimerization of NbAPX3-1. *Myc-NbAPX3-1* and *Flag-NbAPX3-1* were co-expressed in *Nicotiana benthamiana* leaves in the presence or absence of *NbANKr2-GFP* through agroinfiltration. GFP was used as a negative control. Protein complexes were immunoprecipitated with Myc-Trap beads, and the bound protein was detected by immunoblot with indicated antibodies. Three independent experiments were conducted and yielded similar results. (b, c) Luciferase complementation assay indicates the effect of NbANKr2 on the dimerization of NbAPX3-1. *NbAPX3-1-nLuc* and *cLuc-NbAPX3-1* were co-expressed in *N. benthamiana* leaves in the presence or absence of *Flag-NbANKr2* through agroinfiltration. Flag-GFP was used as a negative control. Photograph was taken (b) and quantification of the luciferase signals was analyzed using PlantView100 software, data ($n = 15$) were analyzed from three independent experiments (c). The relative LUC activity of the control group was set to 1. Values represent the means \pm SD. Asterisks represent significance: ***, $P < 0.001$ (Student's *t*-test). (d) Effect of NbANKr2 on protein accumulation of NbAPX3-1. Total proteins were extracted from leaves at 2 and 3 d after agroinfiltration for immunoblots with anti-GFP and anti-Flag antibodies, respectively. The band intensities of Flag-NbAPX3-1 were determined by the gray values using IMAGEJ. Numbers on top of the immunoblot indicate fold changes normalized to the control band intensity (2 d after agroinfiltration), which was set to 1. Three independent experiments were performed and yielded similar results. (e, f) Silencing of *NbANKr2* compromised *NbAPX3-1*-mediated resistance. *EV* and *Flag-NbAPX3-1* were agroinfiltrated into the right and left sides of *TRV-GUS* and *TRV-NbANKr* leaves. Three days after infiltration, the leaves were challenged with mycelium plugs of Pp016. The disease expansion was visualized by trypan blue staining as shown in (e), and the lesions diameters in (f) were measured at 48 h post inoculation, data (*TRV-GUS*, $n = 24$; *TRV-NbANKr*, $n = 27$) were calculated from three independent experiments. Upper quartile, median, and lower quartile values are indicated in each box plot, while the bars outside the box indicate the maximum and minimum values. Asterisks above the bars indicate significant differences: *, $P < 0.05$; ns, no significance (Student's *t*-test). Three independent experiments were performed and yielded similar results.

P. parasitica relative to the negative control EV, as shown by smaller lesions (Fig. 6e,f). However, in the *TRV-NbANKr* plants, the lesion sizes were similar between *Flag-NbAPX3-1* and

EV-overexpressed leaves (Fig. 6e,f), indicating that the NbAPX3-1-mediated plant immunity requires NbANKr2. The expression and integrity of *Flag-NbAPX3-1* and *EV* in the *TRV-NbANKr*

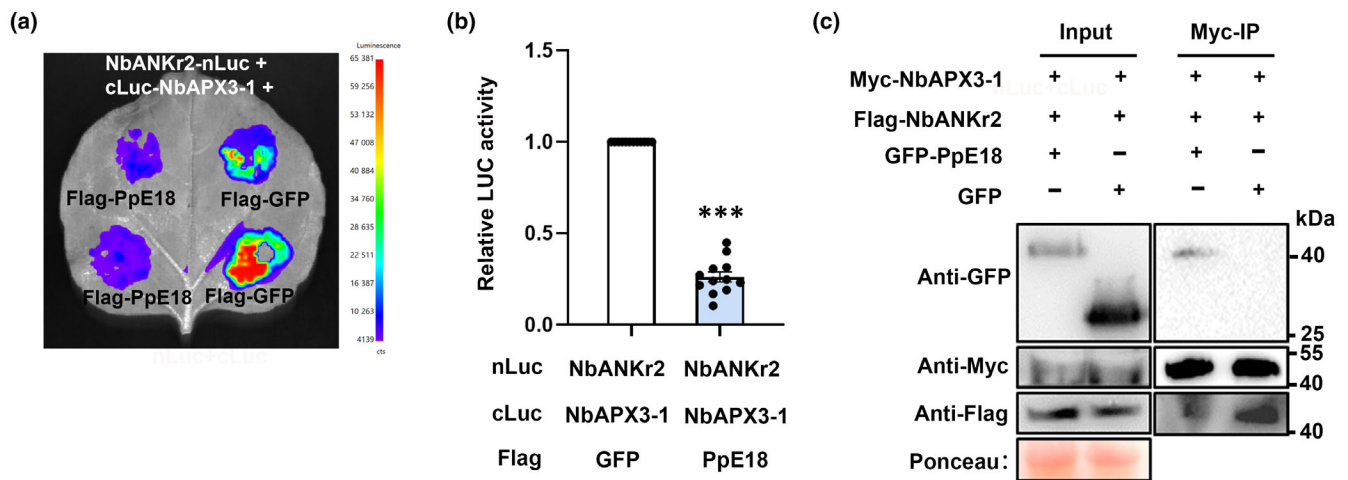


Fig. 7 PpE18 interferes with the interaction between NbAPX3-1 and NbANKr2. (a, b) Luciferase complementation assay to determine the effect of PpE18 on the interaction between NbAPX3-1 and NbANKr2. *NbANKr2-nLuc* and *cLuc-NbAPX3-1* were co-expressed in *Nicotiana benthamiana* leaves in the presence or absence of *Flag-PpE18* through agroinfiltration. *Flag-GFP* was used as a control. The photographs were taken (a), and the quantification of the luciferase signals was analyzed by the PlantView100 software, data ($n = 12$) were analyzed from three independent experiments (b). The relative LUC activity of control group was set to 1. Values represent the means \pm SD. Asterisks represent significance: ***, $P < 0.001$ (Student's *t*-test). (c) Co-IP assay shows the effect of PpE18 on the interaction between NbAPX3-1 and NbANKr2. *Myc-NbAPX3-1* and *Flag-NbANKr2* were co-expressed in *N. benthamiana* leaves in the presence or absence of *GFP-PpE18* through agroinfiltration. GFP was used as a negative control. Protein complexes were immunoprecipitated with Myc-Trap beads, and the bound protein was detected by immunoblot with indicated antibodies. Three independent experiments were performed and yielded similar results.

and TRV-*GUS* leaves were confirmed by western blot (Fig. S21). These findings indicate that NbAPX3-1-mediated disease resistance requires *NbANKr2*, which promotes NbAPX3-1 dimerization and stability.

PpE18 interferes with the interaction between NbAPX3-1 and NbANKr2

Based on our finding that NbANKr2 is necessary for *NbAPX3-1*-mediated disease resistance, we investigated whether PpE18 promotes pathogen infection by interfering with the interaction between NbAPX3-1 and NbANKr2. Co-IP and GST pull-down assays were performed to confirm the interactions between PpE18 and NbANKr2 *in vivo* and *in vitro* (Fig. S18). The results showed that NbANKr2 directly interacted with both NbAPX3-1 and PpE18.

To analyze potential competitive binding between PpE18, NbAPX3-1, and NbANKr2, we co-expressed *cLuc-NbAPX3-1* and *NbANKr2-nLuc* in *N. benthamiana* leaves by agroinfiltration in the presence or absence of *Flag-PpE18*, with *Flag-GFP* as a negative control. Luciferase complementation assay showed that the interaction intensity of NbAPX3-1-NbANKr2 was significantly decreased in the presence of PpE18 (Fig. 7a,b), suggesting that PpE18 might disrupt the interaction between NbAPX3-1 and NbANKr2. To further verify this result, we co-expressed *Myc-NbAPX3-1* and *Flag-NbANKr2* in *N. benthamiana* leaves in the presence or absence of *GFP-PpE18*, followed by pulling down the protein complexes with Myc-Trap beads. The results showed that the band intensity of *Flag-NbANKr2* was decreased in the presence of PpE18 (Fig. 7c). Consistently, we co-expressed *GFP-PpE18* and *Flag-NbANKr2* in the *NbAPX3-1*-silenced

plants, Co-IP assay showed that the band intensity of NbANKr2 was increased in the *NbAPX3-1*-silenced plants compared with that in the TRV-*GUS* plants (Fig. S22). Altogether, these data demonstrated that PpE18 competitively interferes with the interaction between NbAPX3-1 and NbANKr2 in plant cells (Fig. 8).

Discussion

The battle between plants and pathogens resembles an endless arms race. Effectors of pathogens often manipulate plant immunity by targeting host proteins (He *et al.*, 2018; Du *et al.*, 2021; Yang *et al.*, 2021). However, a limited number of virulence effectors in *P. parasitica* have been characterized (Dalio *et al.*, 2018; Huang *et al.*, 2019). In this study, we identified a conserved RXLR effector PpE18 in *P. parasitica*, which was highly up-regulated at early infection stages, and significantly inhibited plant immune responses. Further research revealed that PpE18 targeted two positive immune regulators, the ascorbate peroxidase NbAPX3-1 and the ankyrin repeat-containing protein NbANKr2, providing insights into the virulence mechanism of PpE18.

Plant APX, an important enzyme for H_2O_2 scavenging, is essential for maintaining cellular H_2O_2 homeostasis (Li, 2023). As the APX function of NbAPX3-1 was previously unreported, we confirmed the ROS-scavenging ability of NbAPX3-1 *in vivo* and *in vitro* (Fig. 4a-f). We demonstrated that *P. parasitica* effector PpE18 targeted NbAPX3-1 to manipulate immune responses. This observation is consistent with previous reports that pathogens effectors promote infection by targeting ROS-associated proteins directly or indirectly. Among these, some pathogens utilize negative regulators of plant immunity (Gao *et al.*, 2021; Du

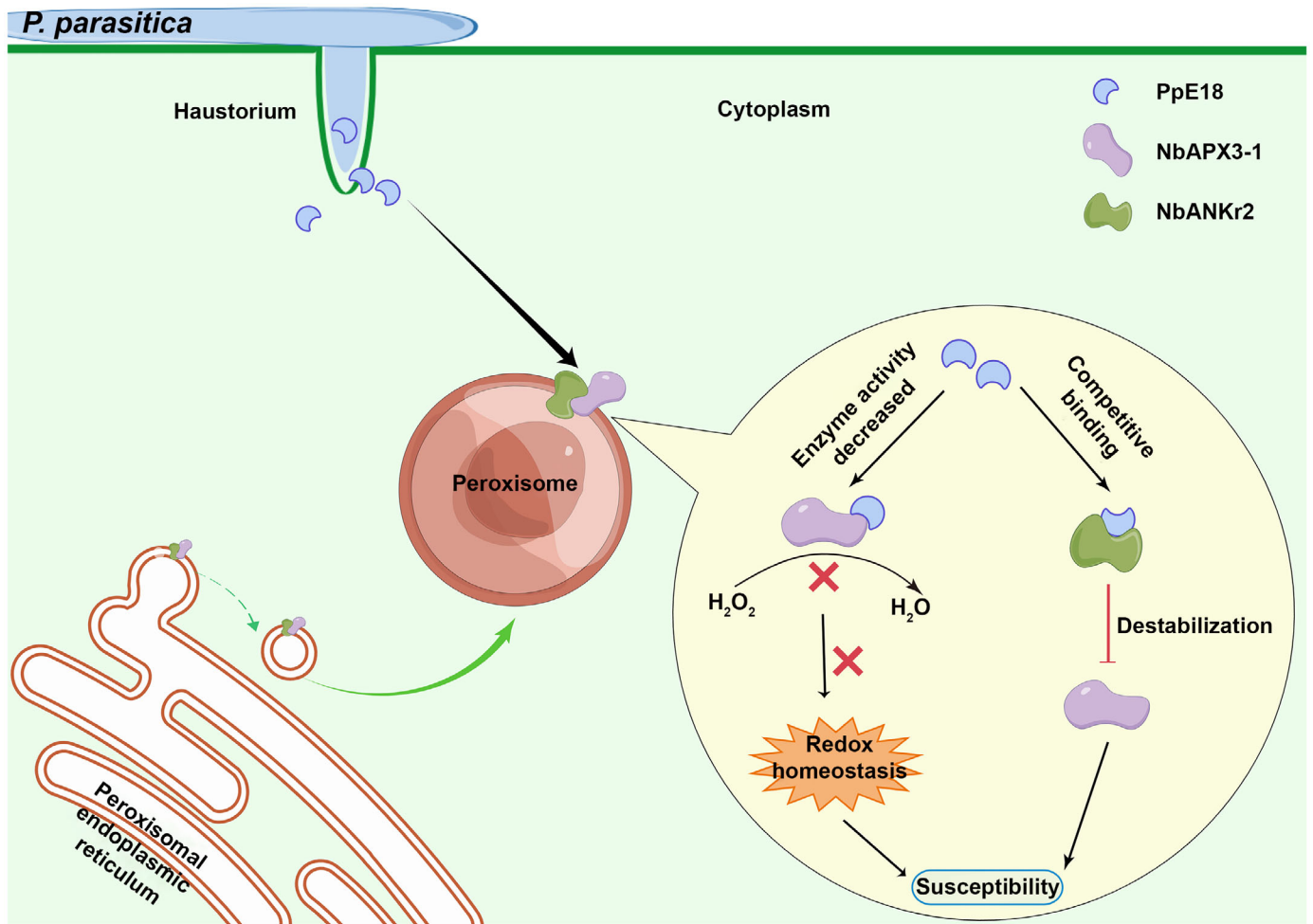


Fig. 8 A working model for the function of PpE18 during *Phytophthora parasitica* infection. In plants, a class of peroxisomal membrane proteins is first targeted to the peroxisomal endoplasmic reticulum (pER), a process that requires ATP and molecular chaperone, and then sorted into peroxisomes via pER-derived vesicles (Mullen *et al.*, 1999; Titorenko & Rachubinski, 2008). NbAPX3-1 was found in both ER and peroxisome membranes and might be targeted to peroxisomes via pER (left bottom). *Phytophthora parasitica* RXLR effector PpE18 is secreted and targeted to the peroxisome membrane of host cells. It interacts with NbAPX3-1 and suppresses reactive oxygen species (ROS)-scavenging activity, causing increased ROS levels within the peroxisome. This disruption of cellular homeostasis may create a more favorable environment for *P. parasitica* infection. Additionally, PpE18 competitively interferes with the interaction between NbAPX3-1 and NbANKr2 by binding to NbANKr2, thereby disturbing the immune function of NbAPX3-1 during infection.

et al., 2023) or disturb positive regulators of ROS levels (Ai *et al.*, 2021) to suppress plant resistance by reducing ROS levels. Therefore, ROS is mostly considered as a positive regulator of plant defense. However, many plant antioxidant enzymes are positive regulators of resistance. CATs contribute to resistance against *P. capsici* in *N. benthamiana* (Zhang *et al.*, 2015). GmCAT1 can mildly induce cell death in *N. benthamiana* and positively regulate plant resistance to *P. sojae* (Zhu *et al.*, 2023). Overexpression of *ZmAPX1* in maize exhibited increased tolerance to *Bipolaris maydis* in part due to decreased H₂O₂ accumulation (Zhang *et al.*, 2022). These examples suggested that positive immune regulators may enhance plant immunity by reducing ROS levels.

NbAPX3-1 was also a major antioxidant enzyme and crucial for resistance to pathogen, as we found that NbAPX3-1 mutant with reduced enzyme activity had reduced resistance to *P. parasitica* (Fig. 4g–i). Moreover, viruses can inhibit antioxidant systems

to increase ROS accumulation, promoting virus accumulation. *Barley stripe mosaic virus* creates an oxidative microenvironment for replication, driving γ b protein to interfere with the NTRC-mediated chloroplast antioxidant system (Wang *et al.*, 2021). Helper component proteinase of *Chilli veinal mottle virus* interacts with CAT1 and CAT3 to inhibit ROS-scavenging activity, facilitating virus infection in *Nicotiana tabacum* (Yang *et al.*, 2020). In our study, we found that PpE18 inhibited the enzymatic activity of NbAPX3-1 *in vivo* and *in vitro*, resulting in increased ROS levels (Fig. 5). The production, transport, and scavenging of ROS in plant cells is in a dynamic balance and is generally maintained at a low level. Under pathogen infection, ROS accumulate rapidly and act as signaling molecules to participate in disease-resistant response. However, redundant ROS can damage cells, and antioxidants are needed to maintain cellular homeostasis (Nanda *et al.*, 2010; Tripathy & Oelmüller, 2012; Noctor *et al.*, 2016). Therefore, we hypothesized that the

stimulation of NbAPX3-1 is involved in fine-tuning the level of H₂O₂, preventing excessive accumulation of ROS, which interferes with cell homeostasis, thereby affecting the normal functioning of the immune system. Pertinently, PpE18 disturbed ROS balance by targeting and inhibiting the enzyme activity of NbAPX3-1.

Ankyrin repeat-containing proteins affect plant growth and development and participate in plant biological processes in response to salt, cold, and oxidative stresses (Cao *et al.*, 2015; Zhang *et al.*, 2016, 2021; Chen *et al.*, 2020; Tang *et al.*, 2022). Additionally, they play important roles in different model plant–pathogen interaction systems (Yan *et al.*, 2002; Vaira *et al.*, 2018). NbANKr2 in *N. benthamiana* containing three ankyrin repeats (Vaira *et al.*, 2018). We found that NbANKr2 contributed to *N. benthamiana* resistance against *P. parasitica* as silencing of *NbANKr2* promotes susceptibility to *P. parasitica*, whereas overexpression of *NbANKr2* enhances *N. benthamiana* resistance (Fig. S20). Furthermore, we showed that NbANKr2 interacted with NbAPX3-1 and was required for NbAPX3-1-mediated disease resistance (Figs 6e,f, S18). These findings highlight the crucial role of NbANKr2 in plant immunity. Moreover, NbANKr2 promoted the dimerization of NbAPX3-1 and increased the protein stability of NbAPX3-1 in *N. benthamiana* (Fig. 6a–d). Emerging evidence has indicated that the dimeric form of the OsAPX2 and AtAPX1 proteins exhibited the highest peroxidase activity (Hong *et al.*, 2018; Kaur *et al.*, 2021). Animal study also found that the active APX existed as dimers rather than monomers by native PAGE analysis (Yuan *et al.*, 2016). We considered that the dimers might be more stable for NbAPX3-1 protein and thus more conducive to its enzyme activity.

Considering that NbANKr2 was required for the disease resistance of NbAPX3-1, and PpE18 interacted with both NbANKr2 and NbAPX3-1 (Fig. S18), we further confirmed that PpE18 influenced the interaction between these two proteins (Fig. 7). Collectively, our study indicates that both NbANKr2 and NbAPX3-1 positively regulate the resistance of *N. benthamiana* to *P. parasitica*, while PpE18 promotes pathogen infection by suppressing biochemical activity and disturbing immune function of NbAPX3-1 (Fig. 8). This will enable a broader understanding of how *Phytophthora* successfully infects plants by targeting diverse cellular components.

Acknowledgements

We thank all the members of our laboratory for their technical assistance and insightful suggestions. This work was supported by the Key Research and Development Plan of Shaanxi Province (2021LLRH-07), National Natural Science Foundation of China (31125022), the Chinese Universities Scientific Fund (2452018044), and the Program of Introducing Talents of Innovative Discipline to Universities (project 111) from the State Administration of Foreign Experts Affairs (B18042).

Competing interests

None declared.

Author contributions

WS, YC, QZ and YM designed the research. YC, QZ, YL, TY and LD performed the experiments and analyzed data. YC, WS, QZ, and YY wrote the manuscript. YC and QZ contributed equally to this work.

ORCID

Yimeng Cao  <https://orcid.org/0009-0008-8475-2977>
Yuan Liu  <https://orcid.org/0009-0009-0251-536X>
Weixing Shan  <https://orcid.org/0000-0001-7286-4041>
Yang Yang  <https://orcid.org/0000-0002-9067-6885>
Qiang Zhang  <https://orcid.org/0000-0002-1711-0914>

Data availability

Sequence data from this article can be found in the NCBI database (<https://www.ncbi.nlm.nih.gov/>) or Sol Genomics Network (<https://www.solgenomics.net/>) under the following accession nos.: PpE18 (PPTG_03535), NbAPX3-1 (Niben101Scf05710g02002.1), and NbANKr2 (Niben101Scf02016g00005.1).

References

- Ai G, Xia Q, Song T, Li T, Zhu H, Peng H, Liu J, Fu X, Zhang M, Jing M. 2021. A *Phytophthora sojae* CRN effector mediates phosphorylation and degradation of plant aquaporin proteins to suppress host immune signaling. *PLoS Pathogens* 17: e1009388.
- Balaban RS, Nemoto S, Finkel T. 2005. Mitochondria, oxidants, and aging. *Cell* 120: 483–495.
- Boller T, Felix G. 2009. A renaissance of elicitors: perception of microbe-associated molecular patterns and danger signals by pattern-recognition receptors. *Annual Review of Plant Biology* 60: 379–406.
- Bustin SA, Vladimir B, Garson JA, Jan H, Jim H, Mikael K, Reinhold M, Tania N, Pfaffl MW, Shipley GL. 2009. The MIQE guidelines: minimum information for publication of quantitative real-time PCR experiments. *Clinical Chemistry* 55: 611–622.
- Cao Y, Chen H, Li Z, Tao J, Ma B, Zhang W-K, Chen S-Y, Zhang J-S. 2015. Tobacco ankyrin protein NEIP2 interacts with ethylene receptor NTHK1 and regulates plant growth and stress responses. *Plant and Cell Physiology* 56: 803–818.
- Chen L, Hu W, Mishra N, Wei J, Hongling L, Yuqi H, Qiu X, Yu S, Wang C, Zhang H *et al.* 2020. AKR2A interacts with KCS1 to improve VLCFAs contents and chilling tolerance of *Arabidopsis thaliana*. *The Plant Journal* 103: 1575–1589.
- Clamp M, Cuff J, Searle S, Barton G. 2004. The Jalview Java alignment editor. *Bioinformatics* 20: 426–427.
- Clough SJ, Bent AF. 1998. Floral dip: a simplified method for *Agrobacterium*-mediated transformation of *Arabidopsis thaliana*. *The Plant Journal* 16: 735–743.
- Dalio RJD, Maximo HJ, Oliveira TS, Dias RO, Breton MC, Felizatti H, Machado M. 2018. *Phytophthora parasitica* effector *PpRxLR2* suppresses *Nicotiana benthamiana* immunity. *Molecular Plant–Microbe Interactions* 31: 481–493.
- Daudi A, O'Brien JA. 2012. Detection of hydrogen peroxide by DAB staining in *Arabidopsis* leaves. *Bio-Protocol* 2: e263.
- Diaz-Vivancos P, Rubio M, Mesonero V, Periago PM, Barcelo AR, Martinez-Gomez P, Hernandez JA. 2006. The apoplastic antioxidant system in *Prunus*: response to long-term plum pox virus infection. *Journal of Experimental Botany* 57: 3813–3824.
- Dong S, Ma W. 2021. How to win a tug-of-war: the adaptive evolution of *Phytophthora* effectors. *Current Opinion in Plant Biology* 62: 102027.

- Du J, Wang Q, Shi H, Zhou C, He J, Wang X. 2023. A prophage-encoded effector from “*Candidatus Liberibacter asiaticus*” targets ASCORBATE PEROXIDASE6 in citrus to facilitate bacterial infection. *Molecular Plant Pathology* 24: 302–316.
- Du Y, Chen X, Guo Y, Zhang X, Zhang H, Li F, Huang G, Meng Y, Shan W. 2021. *Phytophthora infestans* RXLR effector PITG20303 targets a potato MKK1 protein to suppress plant immunity. *New Phytologist* 229: 501–515.
- Eastman S, Smith T, Zaydman MA, Kim P, Martinez S, Damaraju N, DiAntonio A, Milbrandt J, Clemente TE, Alfano JR *et al.* 2022. A phyto-bacterial TIR domain effector manipulates NAD⁺ to promote virulence. *New Phytologist* 233: 890–904.
- Fan G, Yang Y, Li T, Lu W, Du Y, Qiang X, Wen Q, Shan W. 2018. A *Phytophthora capsici* RXLR effector targets and inhibits a plant PPIase to suppress endoplasmic reticulum-mediated immunity. *Molecular Plant* 11: 1067–1083.
- Gao M, He Y, Yin X, Zhong X, Yan B, Wu Y, Chen J, Li X, Zhai K, Huang Y *et al.* 2021. Ca(2+) sensor-mediated ROS scavenging suppresses rice immunity and is exploited by a fungal effector. *Cell* 184: 5391–5404.
- Gou X, Zhong C, Zhang P, Mi L, Li Y, Lu W, Zheng J, Xu J, Meng Y, Shan W. 2022. miR398b and AtC2GnT form a negative feedback loop to regulate *Arabidopsis thaliana* resistance against *Phytophthora parasitica*. *The Plant Journal* 111: 360–373.
- He Q, Naqvi S, McLellan H, Boevink PC, Champouret N, Hein I, Birch PRJ. 2018. Plant pathogen effector utilizes host susceptibility factor NRL1 to degrade the immune regulator SWAP70. *Proceedings of the National Academy of Sciences, USA* 115: E7834–E7843.
- Hong SH, Tripathi BN, Chung MS, Cho C, Lee S, Kim JH, Bai HW, Bae HJ, Cho JY, Chung BY *et al.* 2018. Functional switching of ascorbate peroxidase 2 of rice (OsAPX2) between peroxidase and molecular chaperone. *Scientific Reports* 8: 9171.
- Huang G, Liu Z, Gu B, Zhao H, Jia J, Fan G, Meng Y, Du Y, Shan W. 2019. An RXLR effector secreted by *Phytophthora parasitica* is a virulence factor and triggers cell death in various plants. *Molecular Plant Pathology* 20: 356–371.
- Irieda H, Inoue Y, Mori M, Yamada K, Oshikawa Y, Saitoh H, Uemura A, Terauchi R, Kitakura S, Kosaka A *et al.* 2019. Conserved fungal effector suppresses PAMP-triggered immunity by targeting plant immune kinases. *Proceedings of the National Academy of Sciences, USA* 116: 496–505.
- Jia J, Lu W, Zhong C, Zhou R, Xu J, Liu W, Gou X, Wang Q, Yin J-L, Xu C *et al.* 2017. The 25–26 nt small RNAs in *Phytophthora parasitica* are associated with efficient silencing of homologous endogenous genes. *Frontiers in Microbiology* 8: 773.
- Jiang G, Yin D, Zhao J, Chen H, Guo L, Zhu L, Zhai W. 2016. The rice thylakoid membrane-bound ascorbate peroxidase OsAPX8 functions in tolerance to bacterial blight. *Scientific Reports* 6: 26104.
- Jones JD, Dangl JL. 2006. The plant immune system. *Nature* 444: 323–329.
- Kamoun S. 2006. A catalogue of the effector secretome of plant pathogenic oomycetes. *Annual Review of Phytopathology* 44: 41–60.
- Kaur S, Prakash P, Bak DH, Hong SH, Cho C, Chung MS, Kim JH, Lee S, Bai HW, Lee SY *et al.* 2021. Regulation of dual activity of ascorbate peroxidase 1 from *Arabidopsis thaliana* by conformational changes and posttranslational modifications. *Frontiers in Plant Science* 12: 678111.
- Kumar S, Stecher G, Li M, Knyaz C, Tamura K. 2018. MEGA X: Molecular evolutionary genetics analysis across computing platforms. *Molecular Biology and Evolution* 35: 1547–1549.
- Li S. 2023. Novel insight into functions of ascorbate peroxidase in higher plants: more than a simple antioxidant enzyme. *Redox Biology* 64: 102789.
- Li W, Zhao D, Dong J, Kong X, Zhang Q, Li T, Meng Y, Shan W. 2020. *AtRTP5* negatively regulates plant resistance to *Phytophthora* pathogens by modulating the biosynthesis of endogenous jasmonic acid and salicylic acid. *Molecular Plant Pathology* 21: 95–108.
- Lin Y, Cluette-Brown J, Goodman H. 2004. The peroxisome deficient *Arabidopsis* mutant *ssl1* exhibits impaired fatty acid synthesis. *Plant Physiology* 135: 814–827.
- Liu T, Ye W, Ru Y, Yang X, Gu B, Tao K, Lu S, Dong S, Zheng X, Shan W *et al.* 2011. Two host cytoplasmic effectors are required for pathogenesis of *Phytophthora sojae* by suppression of host defenses. *Plant Physiology* 155: 490–501.
- Liu Y, Schiff M, Dinesh-Kumar SP. 2002a. Virus-induced gene silencing in tomato. *The Plant Journal* 31: 777–786.
- Liu Y, Schiff M, Marathe R, Dinesh-Kumar SP. 2002b. Tobacco Rar1, EDS1 and NPR1/NIM1 like genes are required for N-mediated resistance to tobacco mosaic virus. *The Plant Journal* 30: 415–429.
- Meyer AJ, Brach T, Marty L, Kreye S, Rouhier N, Jacquot J-P, Hell R. 2007. Redox-sensitive GFP in *Arabidopsis thaliana* is a quantitative biosensor for the redox potential of the cellular glutathione redox buffer. *The Plant Journal* 52: 973–986.
- Mullen RT, Lisenbee CS, Miernyk JA, Trelease RN. 1999. Peroxisomal membrane ascorbate peroxidase is sorted to a membranous network that resembles a subdomain of the endoplasmic reticulum. *The Plant Cell* 11: 2167–2185.
- Mullen RT, Trelease RN. 2000. The sorting signals for peroxisomal membrane-bound ascorbate peroxidase are within its C-terminal tail. *Journal of Biological Chemistry* 275: 16337–16344.
- Mullen RT, Trelease RN. 2006. The ER-peroxisome connection in plants: Development of the “ER semi-autonomous peroxisome maturation and replication” model for plant peroxisome biogenesis. *Biochimica et Biophysica Acta* 1763: 1655–1668.
- Nakano Y, Asada K. 1981. Hydrogen peroxide is scavenged by ascorbate-specific peroxidase in spinach chloroplasts. *Plant and Cell Physiology* 22: 867–880.
- Nanda AK, Andrio E, Marino D, Pauly N, Dunand C. 2010. Reactive oxygen species during plant-microorganism early interactions. *Journal of Integrative Plant Biology* 52: 195–204.
- Noctor G, Mhamdi A, Foyer C. 2016. Oxidative stress and antioxidative systems: Recipes for successful data collection and interpretation. *Plant, Cell & Environment* 39: 1140–1160.
- Patterson WR, Poulos TL. 1995. Crystal structure of recombinant pea cytosolic ascorbate peroxidase. *Biochemistry* 34: 4331–4341.
- Ratcliff F, Martin-Hernandez AM, Baulcombe DC. 2001. Technical Advance. Tobacco rattle virus as a vector for analysis of gene function by silencing. *The Plant Journal* 25: 237–245.
- Raven EL. 2000. Peroxidase-catalyzed oxidation of ascorbate. Structural, spectroscopic and mechanistic correlations in ascorbate peroxidase. *Sub-Cellular Biochemistry* 35: 317.
- Ribeiro CW, Korbes AP, Garighan JA, Jardim-Messeder D, Carvalho FEL, Sousa RHV, Caverzan A, Teixeira FK, Silveira JAG, Margis-Pinheiro M. 2017. Rice peroxisomal ascorbate peroxidase knockdown affects ROS signaling and triggers early leaf senescence. *Plant Science* 263: 55–65.
- Sang Y, Macho AP. 2017. Analysis of PAMP-triggered ROS burst in plant immunity. *Methods in Molecular Biology* 1578: 143–153.
- Sarwar S, Kim EN, Kim YJ, Ok SH, Kim KD, Hwang BK, Shin JS. 2005. Overexpression of a pepper ascorbate peroxidase-like 1 gene in tobacco plants enhances tolerance to oxidative stress and pathogens. *Plant Science* 169: 55–63.
- Schneider CA, Rasband WS, Eliceiri KW. 2012. NIH Image to IMAGEJ: 25 years of image analysis. *Nature Methods* 9: 671–675.
- Sharp KH, Mewies M, Moody PCE, Raven EL. 2003. Crystal structure of the ascorbate peroxidase–ascorbate complex. *Nature Structural Biology* 10: 303–307.
- Shen G, Kuppu S, Venkataramani S, Wang J, Yan J, Qiu X, Zhang H. 2010. ANKYRIN REPEAT-CONTAINING PROTEIN 2A is an essential molecular chaperone for peroxisomal membrane-bound ASCORBATE PEROXIDASE3 in *Arabidopsis*. *The Plant Cell* 22: 811–831.
- Sousa RH, Carvalho FE, Ribeiro CW, Passaia G, Cunha JR, Lima-Melo Y, Margis-Pinheiro M, Silveira JA. 2015. Peroxisomal APX knockdown triggers antioxidant mechanisms favourable for coping with high photorespiratory H₂O₂ induced by CAT deficiency in rice. *Plant, Cell & Environment* 38: 499–513.
- Tang Q, Zhao Y-N, Luo S, Lu S. 2022. AKR2A is involved in the flowering process of *Arabidopsis thaliana*. *Plant Signaling & Behavior* 17: e2100685.
- Tintor N, Pauw M, Rep M, Takken FLW. 2020. The root invading pathogen *Fusarium oxysporum* targets pattern-triggered immunity using both cytoplasmic and apoplastic effectors. *New Phytologist* 227: 1479–1492.
- Titorenko V, Rachubinski R. 2008. Chapter 5 Spatiotemporal dynamics of the ER-derived peroxisomal endomembrane system. *International Review of Cell and Molecular Biology* 272: 191–244.
- Tripathy BC, Oelmüller R. 2012. Reactive oxygen species generation and signaling in plants. *Plant Signaling & Behavior* 7: 1621–1633.

- Tsuda K, Katagiri F. 2010. Comparing signaling mechanisms engaged in pattern-triggered and effector-triggered immunity. *Current Opinion in Plant Biology* 13: 459–465.
- Vaira AM, Lim HS, Baughan G, Gulbranson CJ, Miozzi L, Vinals N, Natilla A, Hammond J. 2018. The interaction of *Lolium latent virus* major coat protein with ankyrin repeat protein NbANKr redirects it to chloroplasts and modulates virus infection. *Journal of General Virology* 99: 730–742.
- Wang J, Zhang H, Allen RD. 1999. Overexpression of an *Arabidopsis* peroxisomal ascorbate peroxidase gene in tobacco increases protection against oxidative stress. *Plant & Cell Physiology* 40: 725–732.
- Wang X, Jiang Z, Yue N, Jin X, Zhang X, Li Z, Zhang Y, Wang X-B, Han C, Yu J *et al.* 2021. *Barley stripe mosaic virus* γ b protein disrupts chloroplast antioxidant defenses to optimize viral replication. *EMBO Journal* 40: e107660.
- Wang Y, Meng Y, Zhang M, Tong X, Wang Q, Sun Y, Quan J, Govers F, Shan W. 2011. Infection of *Arabidopsis thaliana* by *Phytophthora parasitica* and identification of variation in host specificity. *Molecular Plant Pathology* 12: 187–201.
- Wang Y, Tyler BM, Wang Y. 2019. Defense and counterdefense during plant-pathogenic Oomycete infection. *Annual Review of Microbiology* 73: 667–696.
- Waypa G, Marks J, Guzy R, Mungai P, Schriever J, Dokic D, Schumacker P. 2010. Hypoxia triggers subcellular compartmental redox signaling in vascular smooth muscle cells. *Circulation Research* 106: 526–535.
- Wei H-L, Zhang W, Collmer A. 2018. Modular study of the type III effector repertoire in *Pseudomonas syringae* pv. tomato DC3000 reveals a matrix of effector interplay in pathogenesis. *Cell Reports* 23: 1630–1638.
- Yan J, Wang J, Zhang H. 2002. An ankyrin repeat-containing protein plays a role in both disease resistance and antioxidation metabolism. *The Plant Journal* 29: 193–202.
- Yang B, Yang S, Guo B, Wang Y, Zheng W, Tian M, Dai K, Liu Z, Wang H, Ma Z *et al.* 2021. The *Phytophthora* effector Avh241 interacts with host NDR1-like proteins to manipulate plant immunity. *Journal of Integrative Plant Biology* 63: 1382–1396.
- Yang M, Li Z, Zhang K, Zhang X, Zhang Y, Wang X, Han C, Yu J, Xu K, Li D. 2017. *Barley Stripe Mosaic Virus* γ b interacts with glycolate oxidase and inhibits peroxisomal ROS production to facilitate virus infection. *Molecular Plant* 11: 338–341.
- Yang T, Qiu L, Huang W, Xu Q, Zou J, Peng Q, Lin H, Xi D. 2020. *Chilli veinlet mottle virus* HCPro interacts with catalase to facilitate virus infection in *Nicotiana tabacum*. *Journal of Experimental Botany* 71: 5656–5668.
- Yuan X, Rietzschel N, Kwon H, Nuno A, Hanna D, Phillips J, Raven E, Reddi A, Hamza I. 2016. Regulation of intracellular heme trafficking revealed by subcellular reporters. *Proceedings of the National Academy of Sciences, USA* 113: E5144–E5152.
- Zhang D, Wan Q, He X, Ning L, Huang Y, Xu Z, Liu J, Shao H. 2016. Genome-wide characterization of the ankyrin repeats gene family under salt stress in soybean. *Science of the Total Environment* 568: 899–909.
- Zhang F-j, Xie Y-h, Jiang H, Wang X, Hao Y-j, Zhang Z, You C-X. 2021. The ankyrin repeat-containing protein MdANK2B regulates salt tolerance and ABA sensitivity in *Malus domestica*. *Plant Cell Reports* 40: 405–419.
- Zhang J, Jia X, Wang GF, Ma S, Wang S, Yang Q, Chen X, Zhang Y, Lyu Y, Wang X *et al.* 2022. Ascorbate peroxidase 1 confers resistance to southern corn leaf blight in maize. *Journal of Integrative Plant Biology* 64: 1196–1211.
- Zhang M, Li Q, Liu T, Liu L, Shen D, Zhu Y, Liu P, Zhou JM, Dou D. 2015. Two cytoplasmic effectors of *Phytophthora sojae* regulate plant cell death via interactions with plant catalases. *Plant Physiology* 167: 164–175.
- Zhang M, Meng Y, Wang Q, Liu D, Quan J, Hardham A, Shan W. 2012. PnPMA1, an atypical plasma membrane H^+ -ATPase, is required for zoospore development in *Phytophthora parasitica*. *Fungal Biology* 116: 1013–1023.
- Zhang Q, Li W, Yang J, Xu J, Meng Y, Shan W. 2020. Two *Phytophthora parasitica* cysteine protease genes, PpCys44 and PpCys45, trigger cell death in various *Nicotiana* spp. and act as virulence factors. *Molecular Plant Pathology* 21: 541–554.
- Zhou Z, Bi G, Zhou JM. 2018. Luciferase complementation assay for protein-protein interactions in plants. *Current Protocol in Plant Biology* 3: 42–50.
- Zhu X, Guo L, Zhu R, Zhou X, Zhang J, Li D, He S, Qiao Y. 2023. *Phytophthora sojae* effector PsAvh113 associates with the soybean transcription factor GmDPB to inhibit catalase-mediated immunity. *Plant Biotechnology Journal* 21: 1393–1407.

Supporting Information

Additional Supporting Information may be found online in the Supporting Information section at the end of the article.

Fig. S1 Expression pattern of *PpE18* during *Phytophthora parasitica* infection of *Nicotiana benthamiana*.

Fig. S2 Conservation of PpE18 among *Phytophthora parasitica* strains from different regions and hosts.

Fig. S3 *PpE18* is indispensable for *Phytophthora parasitica* infection.

Fig. S4 Protein expression and integrity of GFP-PpE18 in transient expression of *Nicotiana benthamiana* leaves and stable expression of *Arabidopsis* transformants leaves.

Fig. S5 Protein expression and integrity of PpE18, PTS2-mCherry, mCherry-ER, and NbAPX3-1 in *Nicotiana benthamiana*.

Fig. S6 Phylogenetic analysis of APX proteins in *Arabidopsis thaliana* and *Nicotiana benthamiana*.

Fig. S7 PpE18-nLuc interaction with cLuc-NbAPX3-1 revealed by luciferase complementation assay.

Fig. S8 Interaction between PpE18 mutants and NbAPX3-1 detected by Co-IP assays.

Fig. S9 Amino acid sequence alignment of NbAPX3-1, AtAPX3, and GmAPX1.

Fig. S10 Subcellular localization of NbAPX3-1 and NbAPX3-1 mutant proteins in *Nicotiana benthamiana*.

Fig. S11 Interaction between PpE18 and NbAPX3-1 truncated mutants detected by Co-IP assays.

Fig. S12 Protein expression and integrity of NbAPX3-1 and GFP-NbAPX3-1 Δ mPTS in *Phytophthora parasitica* inoculation assay in *Nicotiana benthamiana*.

Fig. S13 Detection of recombinant proteins used in the *in vitro* enzyme activity assays.

Fig. S14 PpE18 does not influence the protein accumulation of NbAPX3-1.

Fig. S15 PpE18 does not influence endogenous APX activity in the peroxisome.

Fig. S16 Expression of proteins used in the *in vivo* enzyme activity assays.

Fig. S17 Amino acid sequence alignment between NbANKr2 and AtAKR2.

Fig. S18 Direct interaction between NbANKr2 and NbAPX3-1 or PpE18.

Fig. S19 Dimerization of NbAPX3-1 was elucidated by Co-IP assay.

Fig. S20 *NbANKr2* positively regulates plant immunity.

Fig. S21 Protein expression and integrity of Flag-NbAPX3-1 in the control (TRV-*GUS*) and *NbANKr*-silenced plants.

Fig. S22 Interaction between PpE18 and NbANKr2 in TRV-*NbAPX3-1* silenced leaves.

Table S1 Primers used in this study.

Table S2 Information of 17 *Phytophthora parasitica* strains for PpE18 sequence analysis.

Table S3 Candidate proteins and putative peptides identified in *Nicotiana benthamiana* transiently overexpressing *PpE18* but not GFP.

Please note: Wiley is not responsible for the content or functionality of any Supporting Information supplied by the authors. Any queries (other than missing material) should be directed to the *New Phytologist* Central Office.